

## REACTION KINETICS OF VERSATILE PEROXIDASE FOR THE DEGRADATION OF LIGNIN COMPOUNDS

<sup>1</sup>Busse, N., <sup>1</sup>D. Wagner, <sup>2</sup>M. Kraume and <sup>1,3,4</sup>P. Czermak

<sup>1</sup>Institute of Bioprocess Engineering and Pharmaceutical Technology,  
University of Applied Sciences Mittelhessen, Giessen, Germany

<sup>2</sup>Department of Chemical and Process Engineering, Technische Universität Berlin, Berlin, Germany

<sup>3</sup>Department of Chemical Engineering, Kansas State University, Manhattan KS, USA

<sup>4</sup>Faculty of Biology and Chemistry, Justus-Liebig-University of Giessen, Giessen, Germany

Received 2013-06-24, Revised 2013-10-03; Accepted 2013-10-22

### ABSTRACT

The H<sub>2</sub>O<sub>2</sub>-dependent degradation of adlerol by a crude versatile peroxidase from *Bjerkandera adusta*, a new ligninolytic enzyme, was investigated. Adlerol (1-(3,4-dimethoxyphenyl)-2-(2-methoxyphenoxy)-1,3-propanediol) is a non-phenolic β-O-4 dimer whose structural architecture represents the most abundant unit (50-65%) of the valuable renewable biopolymer lignin. Lignin removal plays a key role in utilizing lignocellulosic biomass in biorefineries. Steady-state analyses in the μL scale showed saturation kinetics for both, H<sub>2</sub>O<sub>2</sub> and adlerol with quite sensitive response to H<sub>2</sub>O<sub>2</sub>. This was characterized through slow transient states (lag phases) prior steady-state and were enhanced by increasing H<sub>2</sub>O<sub>2</sub> concentration. The major reason for such phenomena was found to be an accumulation of compound III (E<sup>III</sup>) via reaction of compound II (E<sup>II</sup>) with H<sub>2</sub>O<sub>2</sub>; instead with adlerol to the enzyme's ground state E<sup>0</sup> in order to restart another catalytic cycle. As result, the enzyme deviated from its normal catalytic cycle. A corresponding threshold was determined at ≥ 50 μM H<sub>2</sub>O<sub>2</sub> and an adlerol to H<sub>2</sub>O<sub>2</sub> ratio of 15:1 for the given conditions. Furthermore, E<sup>III</sup> did not represent a catalytical dead-end intermediate as it is generally described. By an additional decrease of the adlerol to H<sub>2</sub>O<sub>2</sub> ratio of ca. 3 at the latest, considerable irreversible enzyme deactivations occurred promoted through reaction of E<sup>III</sup> with H<sub>2</sub>O<sub>2</sub>. At a mL scale deactivation kinetics by H<sub>2</sub>O<sub>2</sub> were further examined in dependence on adlerol presence. The course followed a time-dependent irreversible deactivation (two step mechanism) and was diminished in the presence of adlerol. The deactivation could be sufficiently described by an equation similar to the Michaelis-Menten type, competitive inhibited by adlerol. Finally, first estimates of the kinetic parameters v<sub>max</sub>, K<sub>m</sub><sup>S1</sup> (S<sub>1</sub>: H<sub>2</sub>O<sub>2</sub>), K<sub>m</sub><sup>S2</sup> (S<sub>2</sub>: adlerol), k<sub>i</sub><sup>app</sup> and K<sub>i</sub><sup>app</sup> were made. Moreover, the peroxidase reaction mechanism was reviewed and recommendations are given preventing premature enzyme losses.

**Keywords:** Versatile Peroxidase (VP), Lignin Model Compound (LMC), Steady-State Kinetics, Slow Transient States, Deactivation

### 1. INTRODUCTION

Lignin is the only naturally synthesized aromatic biopolymer (Dashtban *et al.*, 2010). Together with the polysaccharides cellulose and hemicellulose, lignin forms a complex lignin-carbohydrate network, well-known as lignocellulose, the major compound (around 50%

(Sánchez, 2009)) of vascular plants (Wong, 2009), i.e. wood or straw. Lignocellulose is the most abundant renewable organic raw material on earth, and based on its main constituents of high value, with an annually production of many billion tons (Villas-Bôas *et al.*, 2002).

Lignocellulosic material is of great interest as feedstock for bio-based industrial products and

**Corresponding Author:** Czermak, P., Institute of Bioprocess Engineering and Pharmaceutical Technology,  
University of Applied Sciences Mittelhessen, Wiesenstrasse 14, 35390 Giessen, Germany

biorefineries. Especially wood is focused on biofuel production of second generation due to several reasons: it is inexpensive, available in large amounts (Stöcker, 2008) (3,300 m<sup>3</sup> felled or otherwise removed roundwood per year worldwide (Ek *et al.*, 2009)) and CO<sub>2</sub> neutral, thus contributing to the reduction of greenhouse gas emissions (Lange, 2007). Furthermore, wood is rich in both carbohydrates cellulose (40-50%) and hemicellulose (24-35%) and in lignin ranging from 18% up to 35% (Howard *et al.*, 2003) offering a variety of products besides the biofuels. Nevertheless, much research and development is still needed for utilizing lignocellulosic biomass (Kamm *et al.*, 2008), such as wood, efficiently. The lignin removal plays a considerable role in this connection, since this step has to be addressed before polysaccharide bioconversion can be tackled. This process is hampered due to the lignin complexity (polydisperse 3D construct (Martínez *et al.*, 2005) causing difficulties in analysis) (Eriksson *et al.*, 1990) and as generally known, its enormous recalcitrance to degradation.

H<sub>2</sub>O<sub>2</sub>-dependent ligninolytic heme peroxidases (POXs) and O<sub>2</sub>-dependent laccases (Lac, EC 1.10.3.2), extracellular enzymes from *Basidiomycetous white-rot fungi* (thus, Class II peroxidases), are the most efficient lignin degraders in nature (Kirk and Farrell, 1987). Compared to Lac, POXs have high redox-potentials (a good overview is given by Torres and Ayala (2010)) receiving “high interest as industrial biocatalysts” (Martínez, 2007), consequently. However, POXs have not yet been implemented at large scale (Torres and Ayala, 2010).

The POXs include lignin peroxidases or ligninases (LiP, EC 1.11.1.14), manganese peroxidases (MnP, EC 1.11.1.13), and versatile peroxidases (VP, EC 1.11.1.16), also known as hybrid peroxidases or lignin-manganese peroxidases, since those enzymes combine LiP and MnP catalytic properties. While LiP is probably the most famous biocatalyst studying delignification processes, VP is a relative new POX and was first interpreted as a MnP in 1996 by Martínez *et al.* and in 2000 by Giardina *et al.* (Ruiz-Dueñas *et al.*, 2009a). In contrast to LiP and MnP, VPs are capable to direct degradation/oxidation of a broad spectrum of persistent substrates (e.g. (non-) phenolic lignin compounds, dyes, such as RB5 and others) meaning without the requirement of mediators (Pogni *et al.*, 2005); an important feature for biotechnological applications. Although VPs are limited available (a major drawback for industrial utilization), they have

still attracted double attention, “as model enzymes and as a source of industrial/environmental biocatalysts”, within the last years (Ruiz-Dueñas *et al.*, 2009a). Nonetheless, research work for delignification concerning VPs are seldom, in particular kinetic studies with non-phenolic lignin model dimers (lignin model compounds (LMC)) containing a β-O-4 linkage. These components are the most frequent structural units in lignin biopolymers ranging from 50% up to 65% (Adler, 1977). Moreover, the cleavage of such LMC is a substantial indicator for enzyme catalyzed lignin depolymerization processes (Tien, 1987; Wong, 2009). β-O-4 dimers are therefore suitable for studying delignification mechanisms in a more or less simplified manner as it will be seen later in the text.

The present work focuses on kinetic investigations based on the degradation of the β-O-4 lignin model dimer adlerol by a new (Jena Bioscience, 2010) crude versatile peroxidase (VP) from *Bjerkandera adusta* as a ligninolytic model peroxidase. All studies were conducted without the need of any mediator (e.g. the non-phenolic monomer veratryl alcohol (VA) or Mn<sup>2+</sup>) or surfactant like Tween. In addition, the pH optimum of reaction was determined and enzyme deactivation by H<sub>2</sub>O<sub>2</sub> depending on adlerol amount was also examined.

Ligninolytic peroxidase assays are generally known to be more complex and difficult to optimize (Sinsabaugh, 2010; German *et al.*, 2011). Prior starting with the experimental description, the paper will therefore be continued by a compact review of the POX reaction mechanism providing basic information for a better understanding and in order to differentiate pure enzymatic from non-enzymatic reactions. For this purpose most background knowledge was received from authors examining horseradish peroxidase (HRP) activity from plants (Class III peroxidases) on appropriate phenolic substrates as well as LiP using mainly VA as substrate; β-O-4 lignin model dimers are also involved as LiP substrates. VA is a second metabolite of *Phanerochaete chrysosporium* and other white-rot fungi (Schoemaker and Piontek, 1996) and thus the mediator of choice for LiP enabling phenolic compound oxidation. Both, LiP and HRP are similar in many characteristics (e.g. the enzyme oxidation states as depicted in **Fig. 1-3**) (Schoemaker, 1990) and are so far the most popular and best studied peroxidases. Moreover, it will be expected that the used VP should be in compliance with a LiP from *P. chrysosporium* at least for ca. 60%

(Ruiz-Dueñas *et al.*, 1999). Consequently, LiP reactions are more concerned for comparison throughout this study than those for MnP. Additionally, MnP is strongly  $Mn^{2+}$ -dependent resulting in Mn-mediated degradation processes.

## 2. THE REACTION MECHANISM

It is widely adopted that the catalytic peroxidase (POX) cycle follows a ping-pong mechanism. In contrast to the classical mechanism, the POX reaction scheme (“common for most heme peroxidases” (Dunford, 2010)) is assumed to be irreversible as sketched in **Fig. 1** in simplified terms. That means, formation of enzyme substrate complexes (e.g. ES) prior reaction product generation can be neglected at this point, since they are assumed to be of fleeting non-detectable existence (Dunford, 1991).

Within its catalytic cycle in **Fig. 1** the enzyme undergoes two fundamental structural changes. First (pathway 1), the reaction will be initiated by hydrogen peroxide ( $H_2O_2$ ) through a pH-independent (within the range of approximately 2-7.5 for a LiP (Andrawis *et al.*, 1988) or 3.5 and 7 for a VP (Pérez-Boada *et al.*, 2005)) two-electron oxidation converting the enzyme from its native resting ferric/ground state ( $E^0$ ) to the so-called compound I ( $E^I$ , first intermediate) (Equation (1)), a protein cation radical (Torres and Ayala, 2010) of strong oxidative power (Arnao *et al.*, 1990b).



k: reaction rate constant; index: pathway number

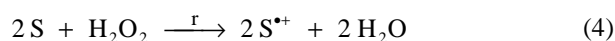
Subsequently,  $E^I$  will be reduced back to the resting state  $E^0$  via a second enzyme intermediate ( $E^{II}$ , compound II) through two consecutive one-electron reduction steps triggered by suitable reducing substrates

(S, the actual electron donor “preferentially electron-rich aromatic compounds” (Lundell *et al.*, 1993a)). Both reaction steps are pH-dependent (Pérez-Boada *et al.*, 2005; Wong, 2009) and causing release of radical cation intermediates ( $S^{*+}$ ) (Palmer *et al.*, 1987) (pathway 3 and 4 in **Fig. 1**, and Equation (2)-(3)):



with  $k_3 \gg k_4$ .

Substrates causing  $E^I$  reduction in Equation (2) can also reduce  $E^{II}$  (Equation (3)) as described by Dunford (2010) for HRP. The same applies for ligninolytic enzymes, such as LiP, and phenolic substrates (Schoemaker, 1990). Hence, the overall net enzyme reaction can be expressed according to Equation (4).



The consumption rate r for S and  $H_2O_2$  can be defined as follows.

$$r = -\frac{1}{2} \frac{d[S]}{dt} = -\frac{d[H_2O_2]}{dt} = \frac{1}{2} \frac{d[S^{*+}]}{dt} \quad (5)$$

However, caution should be exercised with regard to generalization once non-phenolic substrates are involved.

Compound II ( $E^{II}$ ) of LiP can just be reduced by dimethoxylated (minimum amount of alkoxy substituents) non-phenolic aromatic compounds, whereas  $E^I$  also accepts mono-methoxylated aromatic components (Schoemaker, 1990).

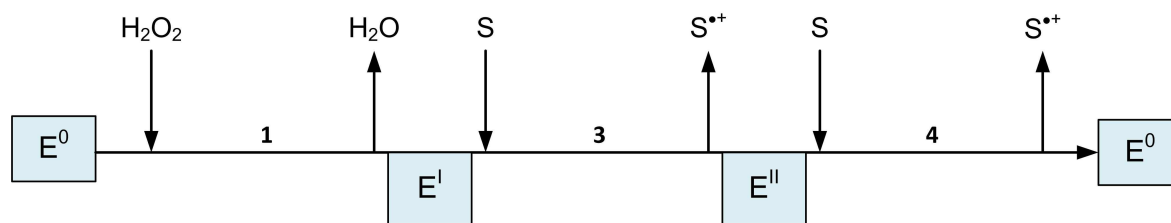


**Fig. 1.** Simplified “POX ping-pong” mechanism.  $E^0$ - $E^{II}$  represents the three main peroxidase oxidation states. The symbols S and  $S^{*+}$  stand for an appropriate substrate (e.g. adlerol) and its corresponding radical cation, respectively. The reaction will be initiated by  $H_2O_2$  (pathway 1) followed by two consecutive one-electron reduction steps (pathway 3-4).

The radical cation intermediates will further pass through non-enzymatic reactions (diffusion controlled) yielding complex mixtures with a wide variety of final products. Depending on the nature of  $S^{*+}$ , the subsequent non-enzymatic reactions include (based on Palmer *et al.* (1987) and Schoemaker (1990)):

- one-electron oxidation of another appropriate substrate molecule (e.g. lignin or lignin derivatives) while  $S^{*+}$  will be reduced to its ground state (S) (Palmer *et al.*, 1987); this reaction is also referred to mediator (diffusible oxidizer) behavior and may be stimulated through rapid electron-transfer from the reducing substrate to  $S^{*+}$  (Schoemaker, 1990)
- $S^{*+}$  may also degrade immediately to a free radical  $R^{\bullet}$  (R also stands for aromatic residual) (Palmer *et al.*, 1987) caused by rapid deprotonation processes (Schoemaker *et al.*, 1994a)
- side-chain cleavage (e.g.  $C\alpha$ - $C\beta$  bond cleavage as seen in **Fig. 2**, C-H bond cleavage)
- demethoxylation
- ether-bond cleavage (e.g. addition of solvent ( $H_2O$ )) (Palmer *et al.*, 1987)
- hydroxylation (e.g. through oxygen incorporation via  $O_2$  or  $H_2O$  from the solvent) of benzylic methylene groups
- phenol formation (by nucleophilic attack, e.g., addition of solvent ( $H_2O$ )) (Palmer *et al.*, 1987)
- aromatic ring cleavage caused by reactions with perhydroxy radicals ( $HOO^{\bullet}$ ; details follow in the next paragraph) (Palmer *et al.*, 1987)

The free-radical species ( $R^{\bullet}$ ) are highly reactive (Palmer *et al.*, 1987) which in turn can bind molecular oxygen ( $O_2$ ) forming the final product and a superoxide anion radical ( $O_2^{\bullet-}$ ) (Schoemaker, 1990) via degradation of an organic peroxy radical intermediate ( $ROO^{\bullet}$ ) (Palmer *et al.*, 1987).  $O_2^{\bullet-}$  undergoes rapid disproportionation to  $H_2O_2$  and  $O_2$  (Harman *et al.*, 1986; Schoemaker, 1990) (**Fig. 3**, Equation (b)). The  $O_2^{\bullet-}$  is in a pH-dependent equilibrium with its protonated counterpart, the perhydroxy radical ( $HOO^{\bullet}$ ) ((Bielski *et al.*, 1985); **Fig. 3**, Equation (a)). At low pH conditions  $HOO^{\bullet}$  predominates and represents a powerful oxidant (Halliwell and Gutteridge, 1985), thus contributing to substrate degradation processes by initiating additional bond cleavage in consequence of substrate (S) oxidation to its radical cation. The oxidant is itself reduced to  $H_2O_2$  (Palmer *et al.*, 1987).

$ROO^{\bullet}$  can react with a further substrate molecule, alternatively, resulting in a new free radical and an organic peroxide ( $ROOR^{\bullet}$ , if R' stands for hydrogen, organic hydroperoxide (ROOH) will be produced) formation (Palmer *et al.*, 1987). Moreover,  $R^{\bullet}$  can undergo dimerization (reaction with other free radicals) as well as polymerization processes (reaction with neutral molecules) (Palmer *et al.*, 1987). In particular, phenolic structures "are prone to polymerize under oxidative conditions" (Schoemaker, 1990).

Free-radical products may also attack the peroxidase along with an inactivation process (Nicell *et al.*, 1993) on the one hand or they act as an additional suitable substrate molecule (thus the radicals can be also considered as S (depending on their chemistry)) for maintaining the catalytic cycle on the other hand. The latter is partly applicable for the radical cation intermediates as discussed later in the text.

Next, the basic adlerol degradation steps, induced by (fungal) heme peroxidases, will be explained aiming to meet the needs of the current study. The graphical illustration is given in **Fig. 2**. Here, the catalytic cycle will be initiated again by  $H_2O_2$  to form  $E^I$ .  $E^I$  further reacts with adlerol (structure I) to  $E^{II}$  and an adlerol cation radical intermediate (structure II) (Lundell *et al.*, 1993b) which will be rapidly fragmented non-enzymatically between its  $C\alpha$ - $C\beta$  bonds in the subsequent (Hatakka *et al.*, 1991). For the latter, various theories have been under consideration.

Based on Tien and Kirk (1984), Kirk *et al.* (1986) and Hatakka *et al.* (1991), the consequence by LiP action is the  $C\alpha$ - $C\beta$  cleavage resulting mainly in veratraldehyde (VAld) (structure IV) formation from the  $C\alpha$  moiety. In parallel, formation of a  $C\beta$ -centred radical (structure VIII) was presumed leading to guaiacol (structure VII) and glycoaldehyde (structure VI) through reaction with  $O_2$  and eventually via an unstable hemiacetal intermediate (structure IX) (Kirk *et al.*, 1986). In general, the reaction course was suggested to be similar to  $\beta$ -1 lignin model compounds (Tien and Kirk, 1984).

In contrast, Lundell *et al.* (1993b) and Schoemaker *et al.* (1994b) concluded a slightly different non-enzymatic reaction after  $C\alpha$ - $C\beta$  cleavage assuming structure II (in **Fig. 2**) with a cation radical centre at the  $C\beta$ -ether oxygen position as consequence of LiP action. They were able to show formation of a veratryl alcohol radical ( $VA^{\bullet}$ , structure III) and a  $C\beta$  cation (structure V) reacting to component IV (preferably), VI and VII, respectively.

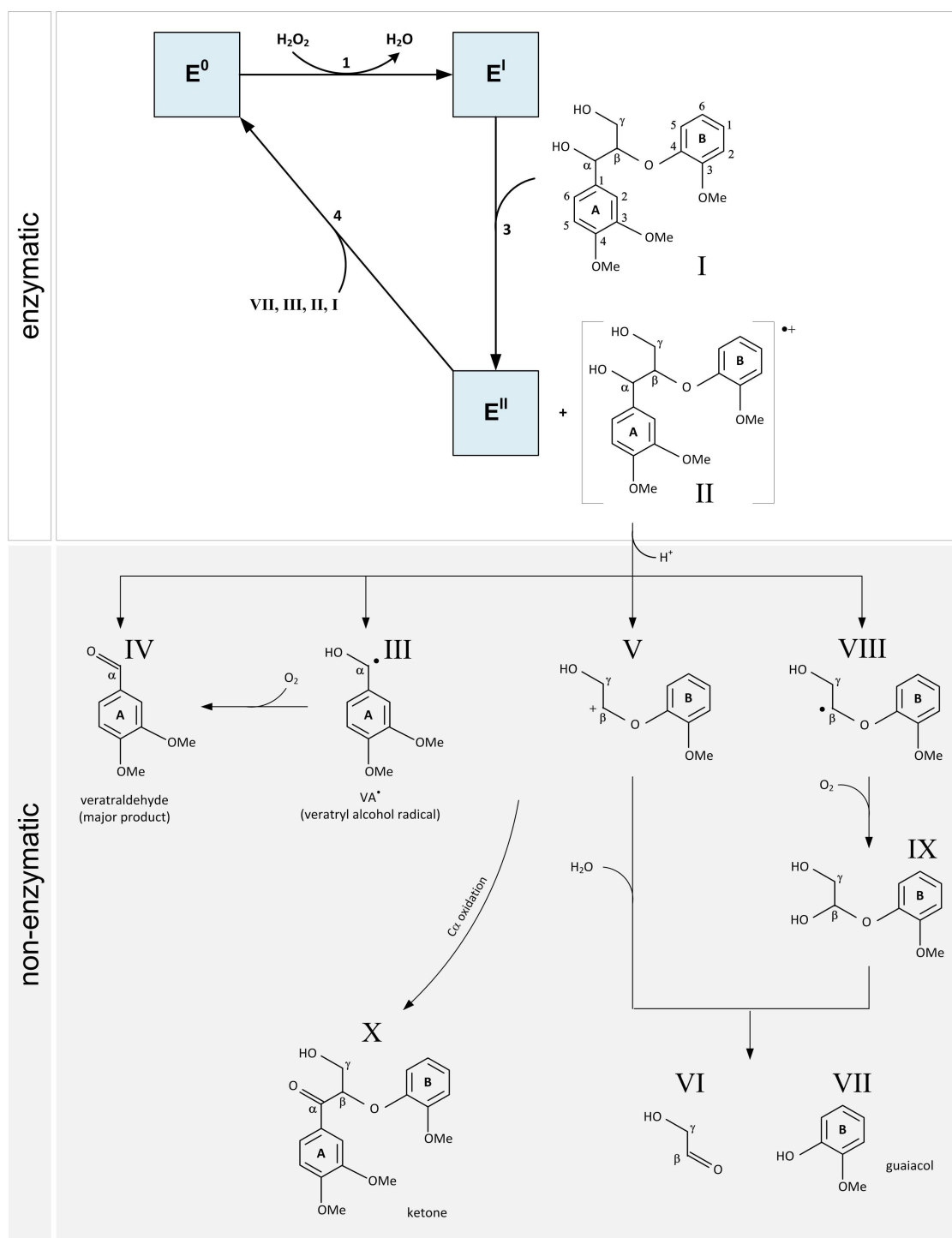


**Fig. 2.** Graphical illustration of the adlerol (β-O-4 model compound, structure I) biocatalysis based on LiP. Several degradation variants (partly in a summarized manner) are shown derived from proposed reaction schemes by Tien and Kirk (1984); Kirk *et al.* (1986); Lundell *et al.* (1993b) and Schoemaker *et al.* (1994b). A detailed description is found in the text.

In addition to the C $\alpha$ -C $\beta$  cleavage, the adlerol cation radical can also undergo C $\alpha$ -oxidation (e.g. due to proton loss (Kirk *et al.*, 1986; Schoemaker, 1990) or direct hydrogen abstraction in the presence of active oxygen species (Snook and Hamilton, 1974) giving rise to a corresponding ketone (structure X, second major product (15%)) generation) (Tien and Kirk, 1984; Kirk *et al.*, 1986). For this purpose, reaction schemes are published by Schoemaker (1990) and by Kirk *et al.* (1986).

Furthermore, some more compounds (e.g. veratrylglycerol) could be detected by Kirk *et al.* (1986), but just in small amounts (thus, these components may be omitted in further analyses). The product distribution is determined by pH, generally (Schoemaker, 1990).

In case adlerol will not serve as reducing substrate any more, for some reason, component III and VII could be act as substrates for driving the cycle back to E<sup>0</sup>. Whereas the reaction with guaiacol (VII) could be monitored, in principle, at 456 nm (Moreira *et al.*, 2006) or at 470 nm as well, due to polymerization (tetraguaiacol (Chance and Maehly, 1955)) of its radical products, apparently phenoxy radicals (Lundell *et al.*, 1993b), the reduction of E<sup>II</sup> to E<sup>0</sup> by component III results finally in veratraldehyde formation (Schoemaker, 1990; Schoemaker *et al.*, 1994b). The latter may only an option under low oxygen conditions (Schoemaker *et al.*, 1994b), since the existence of III is supposed to be short-lived by reacting with O<sub>2</sub> immediately (see discussion above). Remembering the mediator function of radical products component III could cause co-oxidation (thus degradation) of adlerol as well. It is believed that an efficient mediation can only be realized if the degrading substrate will bind close to the active site of the enzyme (Schoemaker *et al.*, 1994b).

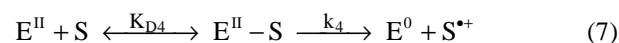
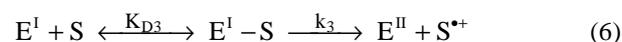
Under substrate (adlerol) limited conditions Tien and Kirk (1984) demonstrated a non-stereospecificity of their used ligninolytic enzyme (LiP) due to complete cleavage of the  $\beta$ -O-4 lignin model compound. This may be an important feature because lignin has a highly irregular (Schoemaker, 1990) structure.

As already indicated above, **Fig. 1 and 2** give just a first insight into the topic. Indeed, the mechanism is far more complex considering certain circumstances (e.g. reaction conditions, enzyme type, presence of inhibitors, substrate and radical chemistry, respectively) as shown schematically in **Fig. 3**. Hence, in the interest of simplification, all POX intermediates are pictured in a more general representation, as already done by several

authors, for this study (due to some structural differences between HRP and ligninolytic enzymes, like VP). In case of the used VP, E<sup>I</sup> and E<sup>II</sup> are expected to be tryptophan radical containing proteins. Thereby, the said tryptophan radical is suggested to be located at the enzymes surface (~ 10-11 Å to the heme centre (Pogni *et al.*, 2005; Ruiz-Dueñas *et al.*, 2009a)) for substrate oxidation purposes. That means, there is no direct contact between the heme (Fe<sup>III</sup>) co-factor and the reducing aromatic substrates, ranging from VA (non-phenolic monomer) up to the complex lignin biopolymer (macromolecule), avoiding steric hindrance. Interactions between substrate and the heme group will be enabled via long range electron transfer (LRET) (Ruiz-Dueñas *et al.*, 2009a). The involvement of LRET in lignin degradation processes through ligninolytic enzymes seems to be generally accepted and can be read up elsewhere.

In the following, a brief explanation will be given for each reaction pathway in **Fig. 3**.

Based on investigation results of transient state kinetics using a recombinant native VP (obtained by *E. coli*), both E<sup>I</sup> and E<sup>II</sup> reduction by VA oxidation exhibited reactions which can be described by Equation (6) and (7) (Ruiz-Dueñas *et al.*, 2009b):



K<sub>D<sub>i</sub></sub> and k<sub><sub>i</sub></sub> (with i = 3,4) are the corresponding equilibrium dissociation constant and rate constant, respectively. That implies, reversible steps (formation of an enzyme-substrate complex or also defined as precursor complex (Dunford, 2010)) are certainly possible within pathway 3 and 4 in **Fig. 1-3**. A reaction behavior similar to Equation (7) was also proposed for the ABTS ([2,2'-azino-bis(3-ethylbenzthiazoline-6-sulfonic acid] diammonium salt) oxidation by a HRP (Smith *et al.*, 1992). As a result, Smith *et al.* (1992) concluded the product dissociation as limiting step, most likely due to good electron donor properties of ABTS which are beneficial for fast precursor complex development.

The two single one-electron oxidations of the substrate S described through Equation (2) and (3) are not universal for peroxidases (Kanofsky, 1991). In case of certain substrates, the two-electron oxidation shown in pathway 9 of **Fig. 3** (van Rantwijk and Sheldon, 2000)

could be dominant as demonstrated with a thyroid peroxidase (TPO) by Nakamura *et al.* (1985).

Furthermore, it seems possible that both, one- and two-electron transfer routes, may occur within a catalytic cycle (Nakamura *et al.*, 1985). For ligninolytic systems, this phenomenon cannot be excluded for sure (this point is also discussed by Schoemaker (1990)). Additionally, an alternative reduction of  $E^{II}$  by radicals (component III), as depicted in **Fig. 2**, makes it difficult to differentiate between two serial one-electron steps and one single two-electron step (Schoemaker, 1990).

However, the most important (side) reactions in the catalytic cycle appear once the S to  $H_2O_2$  ratio is unbalanced (Arnao *et al.*, 1990a; 1990b). It is well-known that the co-substrate  $H_2O_2$  is essential for the catalytic cycle but in excess it will favor reactions diminishing enzyme activity (pathway 5 in **Fig. 3** (Arnao *et al.*, 1990b; Chung and Aust, 1995)) up to enzyme inactivation ( $E_i$ ) (pathway 10, 11 and 13 (Arnao *et al.*, 1990b), and pathway 14 (Wariishi and Gold, 1990)). At low S/ $H_2O_2$  ratios both substrates compete for reactions with  $E^I$  (Tien, 1987; Arnao *et al.*, 1990a) and  $E^{II}$  (Chung and Aust, 1995).

In the event of large  $H_2O_2$  excess or in the absence of a suitable reducing substrate, the POX exhibits time-dependent irreversible inactivation (Vlasits *et al.*, 2010) kinetics (combination of pathway 10, 11 and 13 in **Fig. 3**). Such inactivation is designated as suicide inhibition in the literature belonging to mechanism-based inhibitions. For detailed information the reader is referred to Copeland (2002) and Marangoni (2003). Thereby, the intermediate  $E^I-H_2O_2$  (may also be of fleeting existence (Dunford, 1991)) must not lead exclusively to an inactivated enzyme  $E_i$  (pathway 13). Several pathways are possible.

Concerning the backward reactions first,  $E^I-H_2O_2$  is reversibly dissipated to  $E^I$  (pathway 11) enabling  $H_2O_2$  consumption to  $H_2O$  and  $O_2$  yielding a reduction to  $E^0$  (pathway 2 (Nakajima and Yamazaki, 1987; Valderrama *et al.*, 2002; Vlasits *et al.*, 2010)). Therefore, reaction path 2 is related to catalase activity (Arnao *et al.*, 1990b; Vlasits *et al.*, 2010), whereas Arnao *et al.* (1990b) referred to a direct reaction of  $E^I-H_2O_2$  with  $H_2O_2$  (in the absence of reducing substrate) in this context.  $E^I-H_2O_2$  can also be transformed to  $E^{II}$  (under superoxide anion radical ( $O_2^{\cdot-}$ ) release; pathway 12 (Arnao *et al.*, 1990b)), which will further react with  $H_2O_2$  (pathway 5) to another third intermediate  $E^{III}$  (also defined as compound III) of none or far less catalytic activity (Schoemaker,

1990). This  $E^{III}$  formation will be affected by pH (beside the S/ $H_2O_2$  ratio) and is enhanced at acidic pH values (Cai and Tien, 1992). Finally,  $E^{III}$  becomes either irreversibly inactivated (pathway 14, mediated by further pH-dependent reactions with  $H_2O_2$  (Wariishi and Gold, 1990; Goodwin *et al.*, 1994)) or it decomposes spontaneously (Nakajima and Yamazaki, 1987) under superoxide radical release to the ferric state  $E^0$  (slowly unimolecular reaction, pathway 7 (Arnao *et al.*, 1990b)). Vice versa, Wariishi and Gold (1990) also documented a conversion of  $E^0$  to  $E^{III}$  by  $O_2^{\cdot-}$  in their catalytic scheme with LiP (reverse reaction of pathway 7 (**Fig. 3**)). Alternatively, if reducing substrate is present,  $E^{III}$  returns to  $E^0$  via pathway 6 (reaction is obviously faster than in pathway 7 (Cai and Tien, 1992)) generating a radical cation ( $S^{\cdot+}$ ) (as seen in reaction pathway 3 and 4 (**Fig. 1-Fig. 3**)) and  $H_2O_2$  (Yokota and Yamazaki, 1965; Acosta *et al.*, 1988). Moreover, it is reported that  $E^{III}$  may be converted to  $E^I$  by an one-electron oxidation of S (Tamura and Yamazaki, 1972) as explained through pathway 8. At this point, it has to be mentioned that not all potential POX substrates (S as well as related radicals) are capable to revert  $E^{III}$  (basically to  $E^0$ ) necessarily. Consequently,  $E^{III}$  remains catalytically inactive and will be subjected to oxidative stress due to reactions with  $H_2O_2$ . A practical example for such phenomena is given by Chung and Aust (1995) studying the inactivation of the isozyme H2 of LiP from *P. chrysosporium* by  $H_2O_2$  during phenol oxidation in comparison to VA. They found out that neither the phenolic substrate nor its free-radical product (phenoxyl radical) was competent to convert  $E^{III}$  back to  $E^0$ . The same was observed for VA contrary to its radical cation product ( $VA^{\cdot+}$ ), which reverted  $E^{III}$  to native enzyme as marked by 6' in (**Fig. 3**).

For  $E^{III}$  of HRP's an additional decomposition to  $E^{II}$  was supposed by  $H_2O_2$  dissociation (pathway 19) (Tamura and Yamazaki, 1972; Nakajima and Yamazaki, 1987) through reaction with reducing substrate (Cai and Tien, 1992).

Reconsidering the start-up from the ferric state  $E^0$  in **Fig. 3**, an alternative way was introduced by Acosta *et al.* (1988) (originally worked out by Smith *et al.* (1982)) via direct reaction with substrate S forming the ferrous enzyme ( $E^f$ ) under  $S^{\cdot+}$  release (pathway 15). Depending on the presence of  $O_2$ , two subsequent reaction variants of  $E^f$  may occur. On the one hand  $E^f$  is oxidized to  $E^{III}$  (pathway 16) independent of the  $O_2$  level (Smith *et al.*, 1982; Acosta *et al.*, 1988), on the other hand  $E^f$  will be converted to  $E^{II}$  by  $H_2O_2$  in the absence of  $O_2$  releasing  $H_2O$  (pathway 18) (Jantschko *et al.*, 2005; Dunford, 2010).

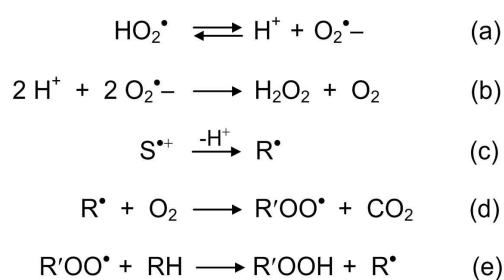
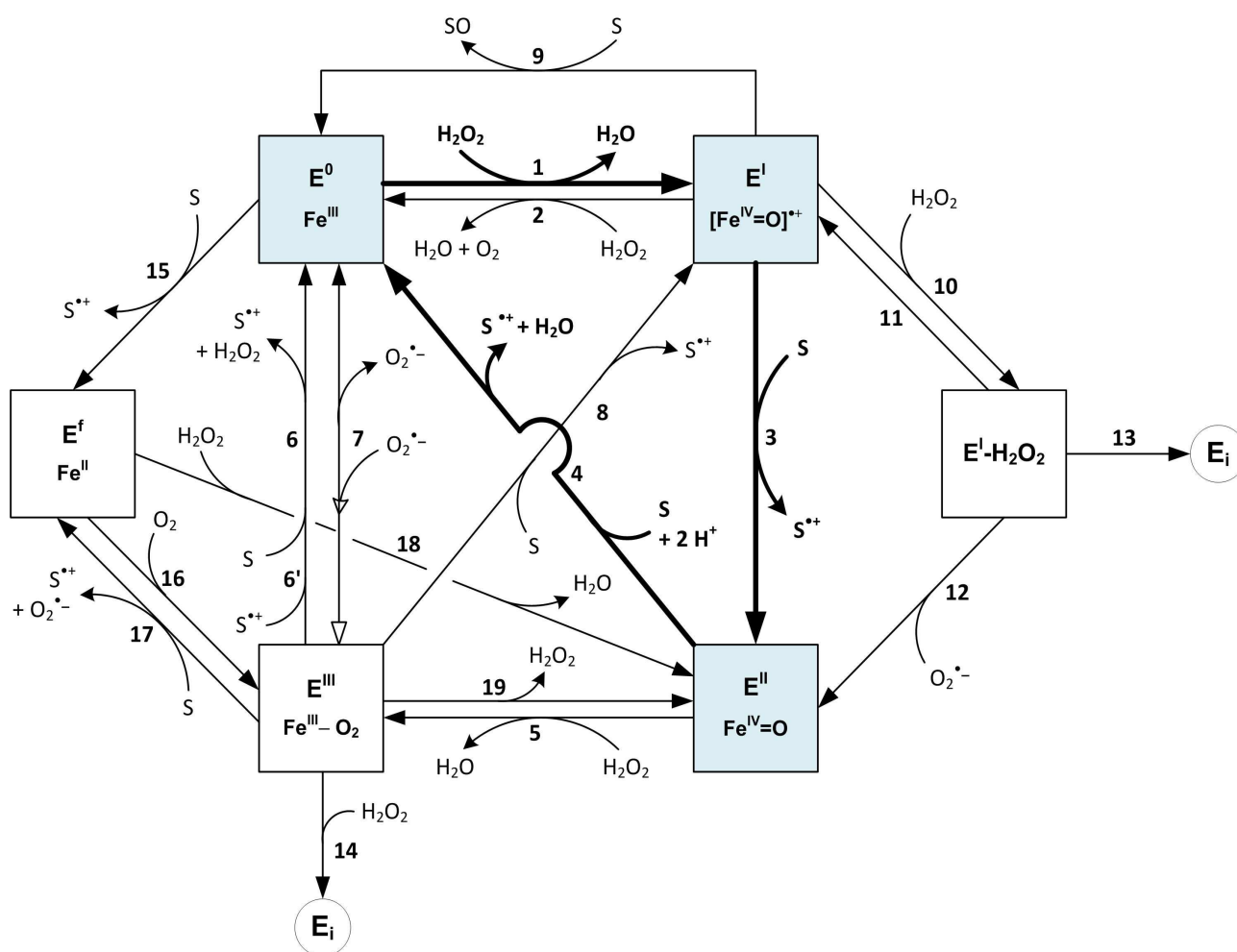
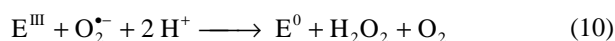
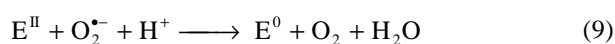


**Fig. 3.** Summary of possible peroxidase intermediates, their development and reaction pathways collected from various research reports containing enzyme reaction studies with horseradish peroxidases and ligninolytic peroxidases (mostly LiP) as well for different reducing substrates. The normal peroxidase cycle is highlighted through bold solid lines while its involved enzyme intermediates are color-shaded. The reaction pathways are numbered (1-19) for identification purposes. The representation of each enzyme intermediate/compound was derived from several authors (Arnao *et al.*, 1990; Schoemaker *et al.*, 1994; Dunford, 2010; Torres and Ayala, 2010) showing formal changes at the heme group. Equation (a)-(e) introduce several important non-enzymatic reactions for completeness, since organic hydroperoxide ROOH competes for reaction with E<sup>0</sup> and E<sup>I</sup>. As a result, enzyme inactivation (pathway 13) occurs (Acosta *et al.*, 1988).

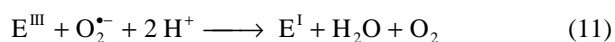
Thus, Acosta *et al.* (1988) gave another option for initiating the catalytic cycle without H<sub>2</sub>O<sub>2</sub> addition. Smith *et al.* (1982) reported also a return of E<sup>III</sup> to E<sup>I</sup> described through pathway 17 (Acosta *et al.*, 1988).

To gain a deeper insight into the structural changes of the enzyme due to reactions shown in **Fig. 3**, the reader is referred to Dunford (1991; 2010) as well as to Torres and Ayala (2010).

Finally, superoxide (or perhydroxyl radicals HO<sub>2</sub><sup>•</sup> at low pH) can be additionally served as electron donor, instead of a reducing substrate. Consequently, all three enzyme states E<sup>I</sup>, E<sup>II</sup> and E<sup>III</sup> may be reduced by O<sub>2</sub><sup>•-</sup> (such unimolecular reactions are omitted in **Fig. 3** for better clarity) under O<sub>2</sub> production (Bielski *et al.*, 1985; Kettle *et al.*, 2007) according to Equation (8)-(11), based on Kettle *et al.* (2007).



or



The reaction in Equation (9) is supposed to prevent enzyme inhibition caused by poor reducing substrates for maintaining its activity (Kettle *et al.*, 2007). In contrast, superoxide and reducing substrate S compete for reactions with the enzyme. Similarly, competition between H<sub>2</sub>O<sub>2</sub> and organic hydroperoxides of the form ROOH (**Fig. 3**, Equation (e)) also exists for reaction with E<sup>0</sup> to E<sup>I</sup> and between S and ROOH for E<sup>I</sup> conversion depending on the relation of their concentrations (reaction pathways are also omitted in **Fig. 3** for more clarity). Reactions of ROOH with E<sup>I</sup> lead to enzyme inactivation. At low O<sub>2</sub> concentrations ROOH formation is limited (Acosta *et al.*, 1988).

In summary, taking the non-enzymatic radical initiated processes above into account, it is evident that even the adlerol degradation mechanism by heme peroxidases is not fully understood and fundamental research work is still needed. The same applies for the conversion of the most studied monomer veratryl

alcohol. This progress is hampered by the systems complexity per se. Nevertheless, veratraldehyde (a stable product, which cannot be further reduced by ligninolytic systems (Kirk *et al.*, 1986)), guaiacol and the Ca keto-form seem to be substantial products of the catalytic POX cycle to work with.

### 3. MATERIALS AND METHODS

In the following all represented concentration data are final concentrations.

#### 3.1. The Enzyme and its Preparation

The heme peroxidase used in this study was a lyophilized crude versatile peroxidase (VP) from *B. adusta*, purchased from Jena Bioscience GmbH, Germany, with a molecular weight (MW) of 43 kDa. The lyophilisate was generally stored at -20°C. For each experiment a fresh VP stock solution, with distilled water as solvent, was prepared directly from the lyophilisate. The Reinheitszahl (RZ) value (ratio heme to total protein content) was sporadically checked by recording the absorbance of 200 µL stock solution at 407 nm (maximum absorption of the heme group or soret band for that VP) and 280 nm (total protein) at room temperature (RT). For this, a HELMA quartz glass microplate (supplied by VWR International GmbH, Germany) and a BioTek microplate reader Synergy HT (BioTek, Germany) was used. The RZ value for the crude VP was 0.3. At least a factor of ten lower, than RZ values for other purified VPs, ranging from 3.2 (Moreira *et al.*, 2006) and 3.5 (Pogni *et al.*, 2005) up to 4.0 (Garcia-Ruiz *et al.*, 2012). However, the RZ value is no indicator for enzymatic activity necessarily (Dunford, 1991; SAC, 2012).

Enzyme activity measurements were carried out according to the instructions, as seen below. Depending on their outcome a further dilution of the enzyme sample to an adequate working solution was required.

With regard to ensuring that enzyme losses could be excluded and the same starting point could be warranted for all studies, respectively, regular enzyme activity measurements of the used VP solution were performed at the beginning as well as at the end of each experimental day. All VP solutions showed persistent activity (1 day) by storing in distilled water at RT.

### 3.2. Preparation of the Co-Substrate Hydrogen Peroxide (H<sub>2</sub>O<sub>2</sub>)

Hydrogen peroxide (30% EMSURE<sup>®</sup> for analysis from Merck KGaA) was purchased from VWR International GmbH, Germany. For each experimental day a suitable stock solution was prepared freshly by diluting the 30% solution with distilled water. To prevent H<sub>2</sub>O<sub>2</sub> consumption, i.e. caused by diverse contaminations or light irradiation, prior enzyme reactions start, the reservoirs needed were cleaned and flushed thoroughly with distilled water before use. Furthermore, the reservoirs were kept sealed, if possible, and the stock solutions were stored in the dark, additionally.

The concentration of each stock solution was controlled by measuring the absorbance at 230 nm ( $\epsilon_{230\text{nm}} = 0.078 \text{ mM}^{-1} \text{ cm}^{-1}$ ) in a HELMA 104-QS semi-micro cuvette SUPRASIL<sup>®</sup> 10.00 mm (obtained from VWR International GmbH, Germany) using a Thermo Spectronic HELIOS  $\Upsilon$  UV-Visible spectrophotometer (Thermo Fisher Scientific, Germany). At random intervals repeated concentration measurements were done for H<sub>2</sub>O<sub>2</sub> stability evaluation. All rechecked solutions were stable.

Depending on the experimental design a further dilution of the stock solution with distilled water to a suitable working solution were also necessary.

### 3.3. Enzyme Activity Measurements

#### 3.3.1 The Assay Procedure

For determining the VP activity, the well-known oxidation reaction of ABTS ([2,2'-azino-bis(3-ethylbenzthiazoline-6-sulfonic acid) diammonium salt] (purchased from AppliChem GmbH, Germany) to the stable green cation-radical ABTS<sup>•+</sup> (Barr and Aust, 1994) was monitored at  $\lambda = 420 \text{ nm}$  according to an internal standard procedure. The assay was carried out in NUNC Immuno-Modules, F8 Polysorp (supplied by VWR International GmbH, Germany) and again on the BioTek microplate reader Synergy HT for the photometric measurements. The reader was operated and programmed through the corresponding data collection and analysis software Gen5<sup>™</sup>, version 1.06.

Each activity test was conducted in sodium acetate buffer at 25°C. The final reaction volume was 200  $\mu\text{L}$  resulting in a layer thickness of 0.57 (determined according to a technical note of Promega (2009)). VP activities were expressed in units (U). Thus, 1 U was

defined as the enzyme amount forming 1  $\mu\text{mol}$  product (ABTS<sup>•+</sup>) from ABTS per minute. The enzyme activity ( $\text{U mL}^{-1}$ ) was calculated using the Gen5 software and its well analysis calculation type Max V, value of the maximum slope (maximal change in absorbance ( $\Delta E$ ) in  $\text{OD min}^{-1}$ ), in Lambert-Beer's law. Every maximum slope was generated from a data set of 8 measuring points along a straight line of  $R^2 \geq 0.998$ .

Each enzyme activity measurement was performed in triplicates. The relative error of the assay was 2-7%.

#### 3.3.2. Preparation of the Sodium Acetate Buffer

The used buffer system was composed of 1 M acetic acid (obtained from 100% acetic acid, EMSURE<sup>®</sup> anhydrous for analysis from Merck KGaA and purchased by VWR International GmbH, Germany) and 1 M sodium hydroxide (made of sodium hydroxide pellets purchased from Carl ROTH GmbH and Co. KG, Germany). The pH was adjusted by titrating with 1 M NaOH while stirring at RT. Finally, the buffer was sterile-filtered with a 0.22  $\mu\text{m}$  PES filter (250 mL polyether sulfone filter from Biochrom AG, Germany) and stored at 2-8°C in the refrigerator until use. For each experimental day the buffer was incubated over night at RT.

#### 3.3.3. Preparation of an ABTS Working Solution

A working solution, varying from 20 to 50 mL in volume according to requirements, was obtained by solving ABTS in distilled water. Finally, it was kept refrigerated (2-8°C) in 1 mL aliquots (1.5 mL Rotilabo<sup>®</sup> reaction vessels for light-sensitive samples from Carl ROTH GmbH and Co. KG, Germany) until use. Under these conditions the working solution is stable at least for one month based on experience. Before each examination the amount of aliquots needed were brought to RT.

### 3.4. The Adlerol Assay for Studying VP Kinetics

#### 3.4.1. The Experimental Procedure

The kinetic assay (modified based on Tien and Kirk (1984)) was carried out in a HELMA quartz glass microplate and on a BioTek microplate reader Synergy HT for monitoring the oxidation product veratraldehyde (VAld) (3,4-dimethoxybenzaldehyde) at  $\lambda = 310 \text{ nm}$  ( $\epsilon_{310} = 9300 \text{ M}^{-1} \text{ cm}^{-1}$  (Tien and Kirk, 1984)) at  $30 \pm 1^\circ\text{C}$ . The reaction mixtures were generally composed of approximately 0.3  $\text{mg mL}^{-1}$  lyophilisate, 0.1 M sodium tartrate buffer (pH 4.0), H<sub>2</sub>O<sub>2</sub> and adlerol varying from

0.015 mM to 0.15 mM and 0.15 mM to 1.5 mM, respectively. For this purpose, the enzyme (0.3 mg mL<sup>-1</sup> final concentration) was pre-incubated first in the microplate reader, together with adlerol and buffer (thus, in an incomplete mixture), at an adjusted temperature of 35°C. The reaction was initiated by H<sub>2</sub>O<sub>2</sub> addition once a temperature of 30°C could be measured in the test solution (external temperature measurement device equipped with a Pt100 sensor from Testo AG, Germany). As a result, 7 min were necessary in principle for pre-incubation.

Preliminary studies have shown that the temperature control unit of the microplate reader has to be adjusted to 35°C in order to maintain a desired temperature of 30±1°C in the reaction mixture with a total volume of 200 µL (resulting in a layer thickness of 0.57 which was determined according to a technical note of Promega (2009)). The actual reaction time and the time interval for recording UV absorption of VALd were 4 min and 10 sec. An enzyme-adlerol mixture (final adlerol concentration varied as seen above) was used as blank.

Controls have taken place previously to evaluate adlerol decay in absence of the VP or H<sub>2</sub>O<sub>2</sub>, respectively. It was found that adlerol could be only degraded to VALd in the presence of both, VP and H<sub>2</sub>O<sub>2</sub>.

All examinations were performed in triplicates. Hence, the reaction velocities (calculations similar to ABTS assay above) were determined as the mean of these three measurements with a maximal standard deviation of ≤ 10% from the mean.

### 3.4.2. Determination of the pH Optimum

The experimental set-up for determining the pH optimum was similar to the kinetic assay. The major differences in this study are the fixed adlerol and H<sub>2</sub>O<sub>2</sub> concentration of 1 mM and 0.1 mM, respectively. In addition, the pH of the 0.1 M sodium tartrate buffer was varied in 0.5 pH units, ranging from 2.0 to 5.0. Buffer solutions were not sterile-filtered because of the direct use after preparation.

### 3.4.3. Preparation of the Sodium Tartrate Buffer

The buffer system, pH 4.0, was made up of 1 M tartaric acid (obtained from L(+) tartronic acid, EMSURE® for analysis from Merck KGaA and purchased by VWR International GmbH, Germany) and 1 M sodium hydroxide, similar to the sodium acetate buffer preparation above.

### 3.4.4. Preparation of an Adlerol Stock Solution

Adlerol (1-(3,4-dimethoxyphenyl)-2-(2-methoxyphenoxy)-1,3-propanediol), with a molecular weight of 334.36 g mol<sup>-1</sup>, was purchased from Wako Chemicals GmbH, Germany (manufacturer is Wako Pure Chemical Industries, Ltd. in Japan). For the kinetic investigations a stock solution was made by solving the required adlerol amount with distilled water containing 10% (v/v) acetone under vigorous stirring for 2-3 h at 35°C. Subsequently, it was stored in a sealed amber glass vial, and in the dark, at RT until use. Under these conditions the adlerol solution is stable at least for one month based on experience.

Depending on examination conditions, the stock solution must be further diluted with distilled water to an appropriate working solution prior starting the experiment.

### 3.5. Set-up for Studying VP Deactivation by H<sub>2</sub>O<sub>2</sub>

Enzyme deactivation studies were conducted in a 10 mL and 50 mL scale, respectively, under continuously stirring with a speed of  $n = ca. 375$  rpm at 30±1°C using a magnetic stirrer of the type MR Hei-Standrad, from Heidolph Instruments GmbH and Co. KG, Germany. For this purpose, an average lyophilisate concentration of 0.06 mg mL<sup>-1</sup> (final concentration with a maximal standard deviation of < 10%) was incubated with H<sub>2</sub>O<sub>2</sub> varying from initially 0 mM up to 1 mM and in the presence (4 mM (10 mL scale)) or absence (50 mL scale) of adlerol. Reaction conditions (buffer system, pH, practical procedure) were similar to those seen in the section above. The reaction was started by enzyme addition and VP stability was determined every three minutes, through the internal ABTS assay, over a time period of 18 min. To this, the measuring time of the ABTS assay has to be modified without affecting signal linearity for reaction velocity determination.

All examinations were performed in duplicates. The remained active enzyme concentration was therefore determined as the mean of these two measurements with a maximal standard deviation of 10% from the mean.

## 4. RESULTS

### 4.1. Effect of pH on VP Reaction Rate

The pH optimum for the H<sub>2</sub>O<sub>2</sub>-dependent adlerol degradation to the major product veratraldehyde (VALd)

by the crude VP from *B. adusta* appeared within the range of 3.5 and 4.0 (Fig. 4).

#### 4.2. Influence of the Pre-incubation Phase with Adlerol

As introduced throughout section “Materials and Methods” the used VP was pre-incubated with adlerol prior each reaction start by H<sub>2</sub>O<sub>2</sub> in order to bring up the reaction temperature to 30°C. The pre-incubation phase was continuously monitored in the incomplete reaction mixture (none H<sub>2</sub>O<sub>2</sub>, thus the final volume was not achieved without causing any considerable impact) by recording the absorption at 310 nm every 10 sec. It was found that the absorption showed saturation behavior while the time course was clearly affected by adlerol concentration, examples are illustrated in Fig. 5. The time required reaching saturation was reduced by an adlerol increase. Furthermore, after saturation was achieved, a relative slow but constant decrease in absorption started; with some time delay at the higher adlerol concentration.

To gain a better understanding of these findings the soret band (heme group absorption maximum of the used VP at 407 nm) was also investigated independently, under equal conditions, at adlerol concentrations of 0 and ca. 1 mM (Fig. 6). Any red or blue shift in the soret band are indicators for changes in the enzyme transition state (E<sup>0</sup>, E<sup>I</sup>-E<sup>III</sup> as well as E<sup>f</sup>). Those shifts are quasi specific and each transition state can be assigned by a certain wavelength, thus enabling the identification of conformational changes of the enzyme under study. For initial orientation, the given characteristic wavelengths for E<sup>0</sup>-E<sup>III</sup> in Table 1 (received from literature) were assumed for this work. Moreover, in order to obtain a representative reference for E<sup>0</sup> and E<sup>III</sup>, the soret band was also examined by storing the VP just in distilled water and 0.1 mM H<sub>2</sub>O<sub>2</sub>, respectively. Both, in the absence of adlerol. On this basis, (notwithstanding the fact that E<sup>II</sup> and E<sup>III</sup> may be difficult to differentiate, which will be further hampered by the chosen buffer system) it is clearly seen in Fig. 6, that the VP was initially in its oxidation state E<sup>III</sup> (by comparing the black dashed solid line with the red ones (VP in H<sub>2</sub>O<sub>2</sub>)) before it was transferred to its ground state E<sup>0</sup> over pre-incubation time; regardless of adlerol presence. This observation is in good agreement with Fig. 5. That means, E<sup>III</sup> spontaneously decayed to E<sup>0</sup>.

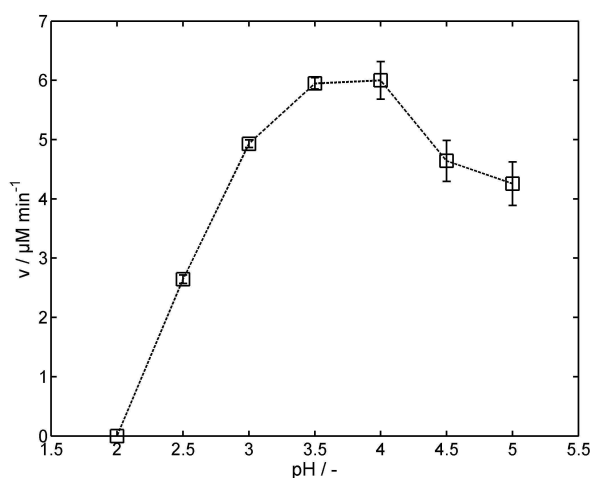


Fig. 4. Effect of the pH on the enzymatic H<sub>2</sub>O<sub>2</sub>-dependent adlerol conversion to veratraldehyde. The studie was performed in triplicates in 100 mM sodium tartrate buffer with 100 μM H<sub>2</sub>O<sub>2</sub>, 1.0 mM adlerol and ca. 0.3 mg mL<sup>-1</sup> VP lyophilisate at 30°C.

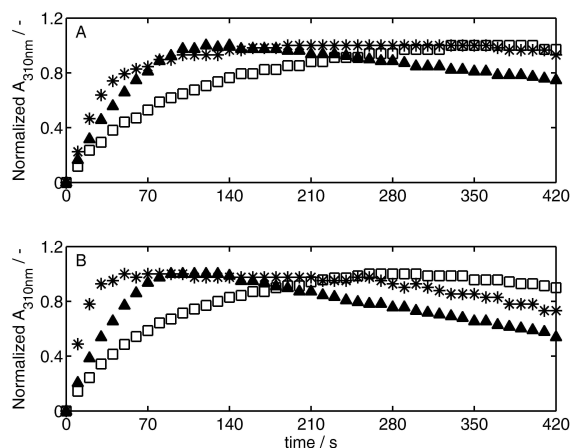


Fig. 5. A-B: Effect of the adlerol amount during pre-incubation. The enzyme was pre-incubated in ca. 100 mM sodium tartrate buffer, pH 4.0 at 0 μM adlerol (reference) (□), 0.13 mM adlerol (▲) and 1.3 mM adlerol (\*). The last two were conducted in 133 mM sodium tartrate buffer, pH 4.0, since the mixtures were without H<sub>2</sub>O<sub>2</sub> and thus, still incomplete in volume.

E<sup>I</sup> (high reactive) and E<sup>f</sup> (as expected for LiP somewhere around 435 nm (Palmer *et al.*, 1987)) could not be detected under the given conditions, or additional peaks within > 500 nm and ≤ 700 nm. An absorption drop of the soret peak at 407 nm with time was also recorded (Fig. 6).

**Table 1.** Assumed solet band maxima of the intermediates E<sup>0</sup>-E<sup>III</sup> for orientation purposes.

Enzyme state	λ nm	Enzyme	Reference
E <sup>0</sup>	407	VP <sup>a</sup>	Pogni <i>et al.</i> (2005)
E <sup>I</sup>	403	rVP <sup>b</sup>	Pérez-Boada <i>et al.</i> (2005)
E <sup>II</sup>	417	rVP <sup>b</sup>	Pérez-Boada <i>et al.</i> (2005)
E <sup>III</sup>	420	LiP <sup>c</sup>	Tien and Kirk (1984)

a. from *Bjerkandera adusta*;

b. recombinant VP from *Escherichia coli*

c. from *Phanerochaete chrysosporium*

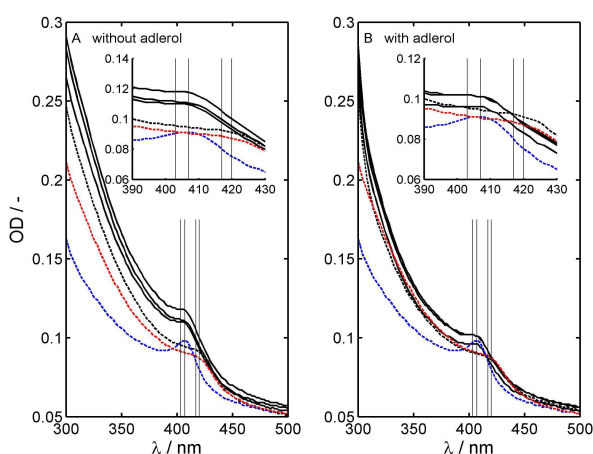


**Fig. 6.** Behavior of the solet band within the first 6 minutes of pre-incubation. A: VP in 100 mM sodium tartrate buffer, pH 4.0, B: VP incubation in an incomplete reaction mixture (without H<sub>2</sub>O<sub>2</sub>) in the presence of ca. 133 mM sodium tartrate buffer, pH 4.0 and ca. 1.3 mM adlerol. The black dashed line represents the starting point of incubation as well as the first wavelength scan (with 2 nm steps) followed by three additional scans with an interval of 2 minutes. The upper black solid line stands for the last scan at time t = 6 minutes. As references, the blue dashed line represents the VP in distilled water, and the red dashed line shows the VP only stored in 0.1 mM H<sub>2</sub>O<sub>2</sub>. The grey lines in the graphs serve only for orientation purposes.

No conformational changes were seen by storing VP in distilled water.

### 4.3. Steady-state Kinetics of the H<sub>2</sub>O<sub>2</sub>-dependent Adlerol Conversion by the Crude VP

The reaction velocities of VALd accumulation obtained throughout the steady-state phase showed a hyperbolic shaped course by varying the H<sub>2</sub>O<sub>2</sub>

concentration at different fixed adlerol concentrations as depicted in **Fig. 7A**. Vice versa, same results were obtained by varying the adlerol concentration at several fixed initial H<sub>2</sub>O<sub>2</sub> concentrations (**Fig. 8A**). Consequently, for each examination procedure two apparent kinetic constants, like the maximum reaction velocity  $v_{\max}^{\text{app}}$  and the dissociation constant  $K_m^{\text{app}}$ , were determined according to the Michaelis-Menten equation type as follows. The index S<sub>i</sub> in Equation (12) stands for the concentration of substrate i, such as H<sub>2</sub>O<sub>2</sub> for i = 1 and adlerol for i = 2.

$$v = \frac{v_{\max}^{\text{app}} [S_i]}{K_m^{\text{app}} + [S_i]}, \quad i = 1, 2 \quad (12)$$

To solve the data-fitting problem in least-square sense the MATLAB<sup>®</sup> non-linear curve fit function 'lsqcurvefit' (default setting) was used resulting in the kinetic constants listed in **Table 2 and 4**. For each calculation, initial starting points for  $v_{\max}^{\text{app}}$  and  $K_m^{\text{app}}$  were estimated from intercepts ( $b = 1/v_{\max}^{\text{app}}$ ) and slopes ( $m = K_m^{\text{app}}/v_{\max}^{\text{app}}$ ), respectively, of the reciprocal plots seen in **Fig. 7B and 8B** by linear regression (general formula:  $y(x) = mx + b$ ). Once, these plots run parallel to each other, ping-pong mechanism exists (Bisswanger, 2008). The plots just partly show parallelism in **Fig. 8B**, whereas those in **Fig. 7B** are nearly parallel.

Note: At an initial H<sub>2</sub>O<sub>2</sub> concentration range of 50 μM to 100 μM H<sub>2</sub>O<sub>2</sub> depletion was reached within ca. 3 min, whereas at 15 μM H<sub>2</sub>O<sub>2</sub> the reaction may be already done after ca. 1.5 min at the latest.

Assuming the POX cycle will be not inhibited and irreversible with  $k_3 \gg k_4$ , while  $k_4$  is just rate limiting (see simplified two substrate (H<sub>2</sub>O<sub>2</sub> and adlerol (S)) scheme in **Fig. 1**), the steady-state product (VALd) accumulation can be simply described by Equation (13) (in consideration of Equation (1)-(5); only with VALd as product). A detailed deduction can be found in the study of Rasmussen *et al.* (1995).

$$\frac{d[\text{VALd}]}{dt} = \frac{2 k_4 [E_T][S_2][S_1]}{\frac{k_4}{k_1} [S_2] + [S_1]} \quad (13)$$

with the reaction rate constant:

$$k_4 = k_{\text{cat}} \quad (14)$$

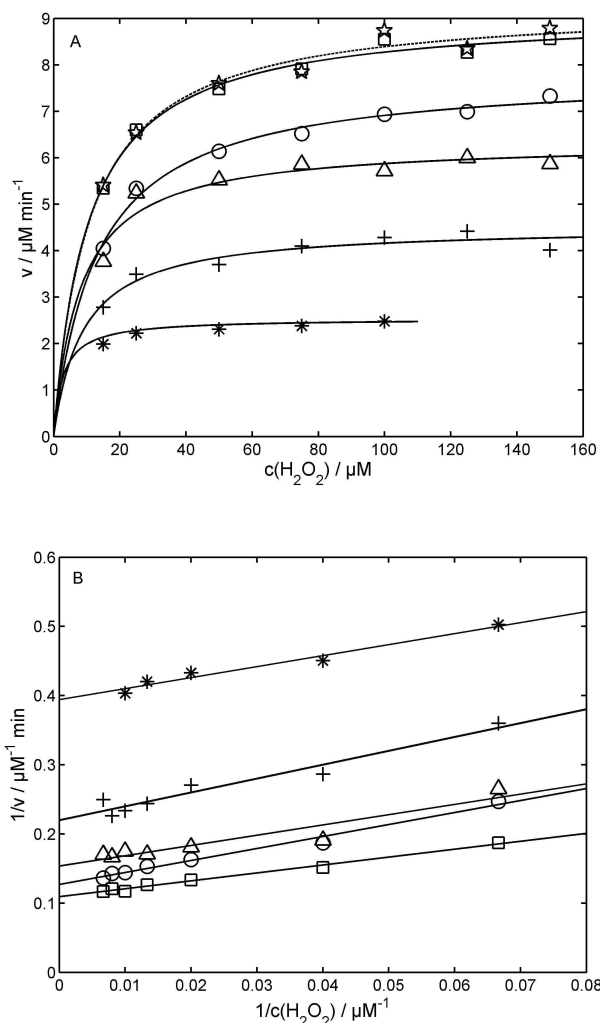


**Fig. 7.** A: VP kinetics for the co-substrate  $\text{H}_2\text{O}_2$  at different constant adlerol concentrations as follows: 100  $\mu\text{M}$  (\*), 250  $\mu\text{M}$  (+), 500  $\mu\text{M}$  ( $\Delta$ ), 750  $\mu\text{M}$  (O), 1000  $\mu\text{M}$  ( $\square$ ), and 1500  $\mu\text{M}$  ( $\star$ ). Reactions were conducted in a 200  $\mu\text{L}$  scale in 100 mM sodium tartrate buffer, pH 4.0, at 30°C and an enzyme concentration of ca. 0.3  $\text{mg mL}^{-1}$ . Computer simulated curves are demonstrated by black solid lines or a dotted black line for  $c(\text{adlerol}) = 1500 \mu\text{M}$ . B: Double-reciprocal plot of the data shown in A. Due to the enormous similarity of the results obtained at fixed 1000  $\mu\text{M}$  adlerol and 1500  $\mu\text{M}$ , the latter was omitted to provide a better overview. The almost parallel arrangement of the straight solid lines (gained through linear regression ( $y = mx + b$ )) indicates a ping-pong bi bi mechanism.

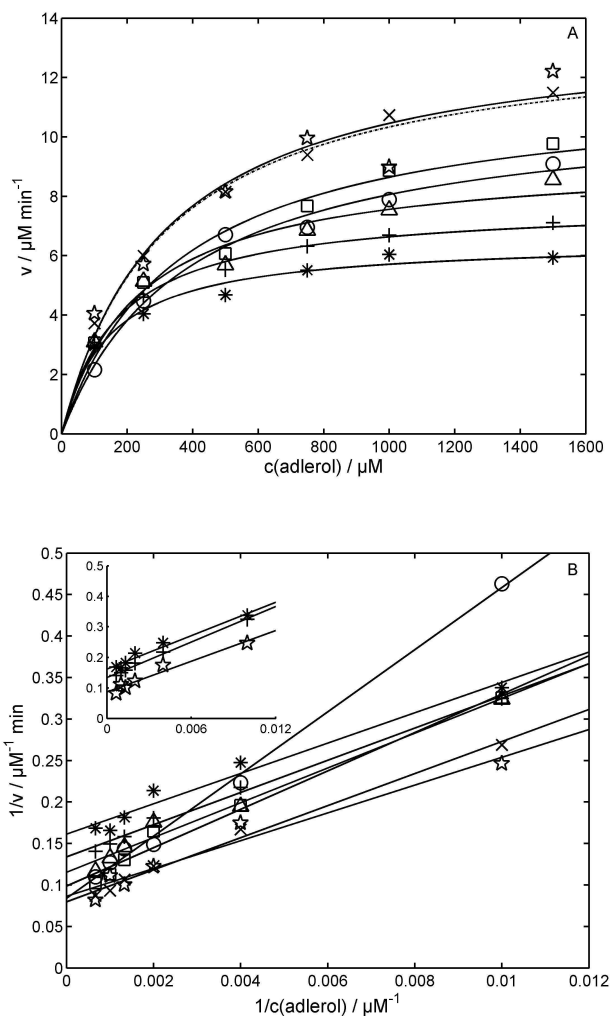


**Fig. 8.** A: VP kinetics for the reducing substrate adlerol at several fixed initial  $\text{H}_2\text{O}_2$  concentrations as follows: 15  $\mu\text{M}$  (\*), 25  $\mu\text{M}$  (+), 50  $\mu\text{M}$  ( $\Delta$ ), 75  $\mu\text{M}$  (O), 100  $\mu\text{M}$  ( $\square$ ), 125  $\mu\text{M}$  ( $\star$ ), and 150  $\mu\text{M}$  ( $\times$ ). Reactions were conducted in a 200  $\mu\text{L}$  scale in 100 mM sodium tartrate buffer, pH 4.0, at 30°C and an enzyme concentration of ca. 0.3  $\text{mg mL}^{-1}$ . Computer simulated curves are demonstrated by black solid lines or a dotted black line for  $c(\text{H}_2\text{O}_2) = 150 \mu\text{M}$ . B: Double-reciprocal plot of the data shown in A. No parallelism is seen in general. The inset plot show the results of linear regression at initial  $\text{H}_2\text{O}_2$  concentrations of 15  $\mu\text{M}$  (\*), 25  $\mu\text{M}$  (+) and 125  $\mu\text{M}$  ( $\star$ ) where parallelism can be observed. The black solid lines are gained through linear regression of the general formula  $y = mx + b$ .

and the enzyme mass balance

$$[E_T] = [E^0] + [E^I] + [E^{II}] \quad (15)$$

The total enzyme concentration  $E_T$  was calculated by assuming 8.6% of the used lyophilisate are the actual VP amount (in consideration of the determined RZ value of 0.3 compared to the reported 3.5 (Pogni *et al.*, 2005)).

Setting

$$A = k_4 [S_2] \quad (16)$$

$$B = \frac{k_4}{k_1} [S_2] \quad (17)$$

(Rasmussen *et al.*, 1995), which is valid and feasible for constant adlerol concentrations (Fig. 7) and rearranging, Equation (13) becomes to Equation (18).

$$\frac{d[VAld]/dt}{2[E_T]} = \frac{A[S_1]}{B + [S_1]} \quad (18)$$

Finally, plots of the coefficients like A vs. B (coefficients were obtained via the same non-linear curve fit approach, as previously discussed using Equation (18)) and A vs. [adlerol] should yield straight lines if the mechanism follows the classical POX cycle and is irreversible (Fig. 1), respectively (Bakovic and Dunford, 1993). As illustrated in Fig. 9, neither plot A nor plot B appears linear. Plot B shows definitely a hyperbola dependence of coefficient A on adlerol, while plot A tends rather towards linearity (but is still not satisfactory following the solid line in plot A of Fig. 9).

By secondary plots of the apparent kinetic parameters  $v_{max}^{app}$  and  $K_m^{app}$  given in Table 2 and 4, both display hyperbolic dependence on adlerol as well as on  $H_2O_2$  concentration (Fig. 10-11), whereas the dissociation constants seem to have a maximum. For adlerol the maximum  $K_m^{app}$  is ca. 382  $\mu M$  at a  $H_2O_2$  concentration of 75  $\mu M$  and for  $H_2O_2$  ca. 13  $\mu M$  at an adlerol concentration of 750  $\mu M$  before decreasing to 319  $\mu M$  and 11  $\mu M$ . Repeated VP reactions at fixed 75  $\mu M$  and 150  $\mu M$   $H_2O_2$  concentrations were done independently and confirmed the findings in Fig. 11.

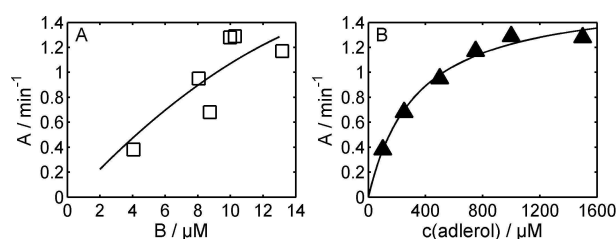


**Fig. 9.** A: Coefficient A vs. coefficient B (both received by non-linear curve fitting using Equation (18)). Non-linear course indicates deviation from the normal POX cycle. Black solid line was just drawn for orientation. B: Hyperbola dependency of coefficient A on adlerol concentration as general indicator for the involvement of reversible (unimolecular) reaction steps. The black solid line in B illustrates computer simulation using a Michaelis-Menten type formula.

However, due to the apparent hyperbolic dependence of the kinetic parameters on both substrates a two substrate ping-pong bi bi mechanism will be suggested with formation of binary enzyme-substrate (ES) complexes before irreversible product release occurs (Marangoni, 2003). The generally accepted non-inhibited rate equation, just concerning forward reaction in the absence of product(s), is given through Equation (19) (Bisswanger, 2008; Cornish-Bowden, 2012).

$$v = \frac{v_{max} [S_1][S_2]}{K_m^{S1} [S_2] + K_m^{S2} [S_1] + [S_1][S_2]} \quad (19)$$

In case  $S_1$  ( $H_2O_2$  concentration) varies and  $S_2$  (adlerol concentration) is treated as constant, which was more realistic for the current study, Equation (19) takes the Michaelis-Menten form seen in Equation (12) (for  $S_1 = S_1$ ) with the parameters  $v_{max}^{app}$  and  $K_m^{app}$  as follows.

$$v_{max}^{app} = \frac{v_{max} [S_2]}{K_m^{S2} + [S_2]} \quad (20)$$

$$K_m^{app} = \frac{K_m^{S1} [S_2]}{K_m^{S2} + [S_2]} \quad (21)$$

By fitting Equation (20) and (21) to the represented data in Fig. 10 using the known non-linear approach, first estimates of the kinetic parameters  $v_{max}$ ,  $K_m^{S1}$  and  $K_m^{S2}$  were made as recorded in Table 3.

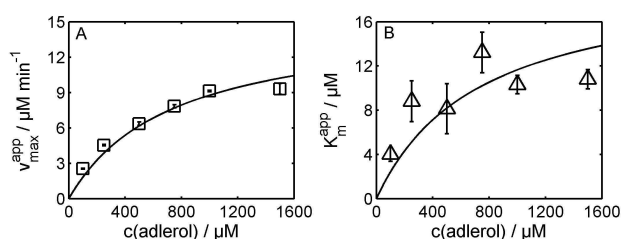


**Fig. 10.**  $v_{\max}^{\text{app}}$  (A),  $K_m^{\text{app}}$  (B) dependence on  $c(\text{adlerol})$ .  $v$  and  $K$  represent the data listed in **Table 2**. The black solid line denotes a computational non-linear curve fit as explained in the text by using Equation (20) (A) and Equation (21) (B).

**Table 2.** Apparent kinetic constants  $v_{\max}^{\text{app}}$  and  $K_m^{\text{app}}$  varying  $\text{H}_2\text{O}_2$  at different fixed adlerol concentrations.

$c(\text{adlerol})$ $\mu\text{M}$	Kinetic constants	
	$v_{\max}^{\text{app}}$ $\mu\text{M min}^{-1}$	$K_m^{\text{app}}$ $\mu\text{M}$
100	$2.5 \pm 0.0$	$4.0 \pm 0.6$
250	$4.5 \pm 0.1$	$8.8 \pm 1.9$
500	$6.4 \pm 0.1$	$8.1 \pm 2.3$
750	$7.8 \pm 0.1$	$13.2 \pm 1.8$
1000	$9.1 \pm 0.1$	$10.3 \pm 0.8$
1500	$9.3 \pm 0.5$	$10.8 \pm 0.9$

The kinetic constants represent the results of a non-linear curve fit using the mean steady-state reaction velocity of three measurements. All reactions were carried out in 100 mM sodium tartrate buffer (pH 4.0) at  $T = 30^\circ\text{C}$ .

**Table 3.** Estimates of  $v_{\max}$ ,  $K_m^{S1}$ , and  $K_m^{S2}$  for constant adlerol conditions ( $S_1$ :  $\text{H}_2\text{O}_2$ ,  $S_2$ : adlerol).

Kinetic parameter	$v_{\max}$ $\mu\text{M min}^{-1}$	$K_m^{S1}$ $\mu\text{M}$	$K_m^{S2}$ $\mu\text{M}$
$[S_2] = \text{constant}$	12.2	16.4	417

Data were calculated by non-linear curve fitting using Equation (20) and (21), respectively.

#### 4.4. Pre-steady-state Transients

Prior steady-state (linear reaction rate velocity has been developed) slow transient phenomena in form of a lag phase appeared once  $\text{H}_2\text{O}_2$  exceeded a certain concentration (**Fig. 12 and 13**).

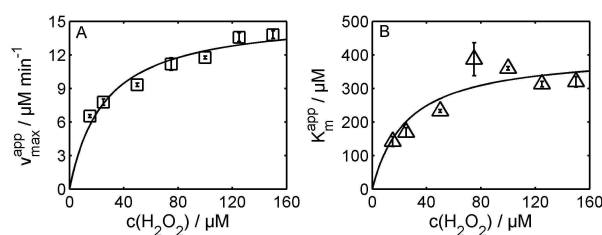


**Fig. 11.** Effect of  $\text{H}_2\text{O}_2$  on  $v_{\max}^{\text{app}}$  (A) and  $K_m^{\text{app}}$  (B).  $v$  and  $K$  represent the data listed in **Table 4**. Black solid lines are just drawn for orientation.

**Table 4.** Apparent kinetic constants  $v_{\max}^{\text{app}}$  and  $K_m^{\text{app}}$  varying adlerol at different fixed initial  $\text{H}_2\text{O}_2$  concentrations.

$c(\text{H}_2\text{O}_2)$ $\mu\text{M}$	Kinetic constants	
	$v_{\max}^{\text{app}}$ $\mu\text{M min}^{-1}$	$K_m^{\text{app}}$ $\mu\text{M}$
15	$6.5 \pm 0.1$	$141 \pm 15$
25	$7.8 \pm 0.3$	$168 \pm 14$
50	$9.3 \pm 0.2$	$233 \pm 4$
75	$11.1 \pm 0.6$	$382 \pm 50$
100	$11.8 \pm 0.1$	$360 \pm 5$
125	$13.6 \pm 0.4$	$313 \pm 8$
150	$13.8 \pm 0.3$	$319 \pm 16$

The kinetic parameters represent the results of a non-linear curve fit using the mean steady-state reaction velocity of three measurements. All reactions were carried out in 100 mM sodium tartrate buffer (pH 4.0) at  $T = 30^\circ\text{C}$ .

Under the current reaction conditions the threshold will be approximately at  $c(\text{H}_2\text{O}_2) \geq 50 \mu\text{M}$ . Based on a constant adlerol concentration (an illustrative example is given in **Fig. 12**), the lag phase was extended by increasing the initial  $\text{H}_2\text{O}_2$  concentration until a maximum is achieved, obviously without affecting the subsequent steady-state velocity  $v$  which supports the data in **Fig. 7A**. Any additional  $\text{H}_2\text{O}_2$  increase led to a drop in absorption signal (absorption of the VP-adlerol blank is greater than that of the full reaction mixture as seen in **Fig. 14**) resulting first in negative reaction rates, apparently of the same initial speed. The negative slope declined with time until it stagnated (a minimum/turning point was reached) before product accumulation could be finally detected. Whereas the time course in **Fig. 14** is strongly dependent on the  $\text{H}_2\text{O}_2$  load until reaching the turning point, the subsequent product accumulation profile remained unaffected.

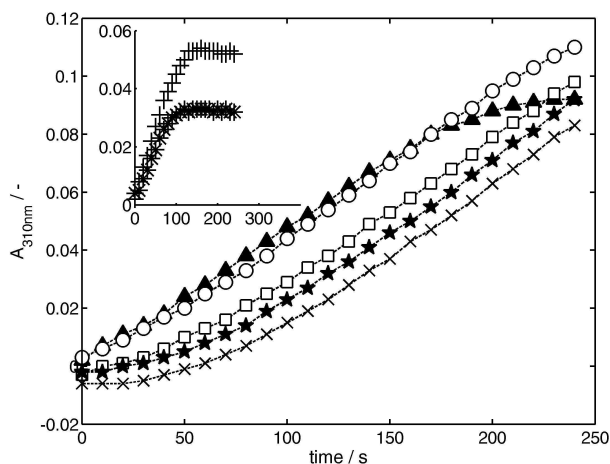


**Fig. 12.** Lag phase formation by increasing the H<sub>2</sub>O<sub>2</sub> amount (50 μM (▲), 75 μM (○), 100 μM (□), 125 μM (★), and 150 μM (×); inset plot: 15 μM (\*), 25 μM (+)) at a fixed adlerol concentration of 500 μM. The corresponding adlerol to H<sub>2</sub>O<sub>2</sub> ratios are 33.3, 20, 10, 6.7, 5, 4, and 3.3. The absorption value (data are already corrected by blank) at a wavelength of 310 nm is plotted as a function of measuring time.

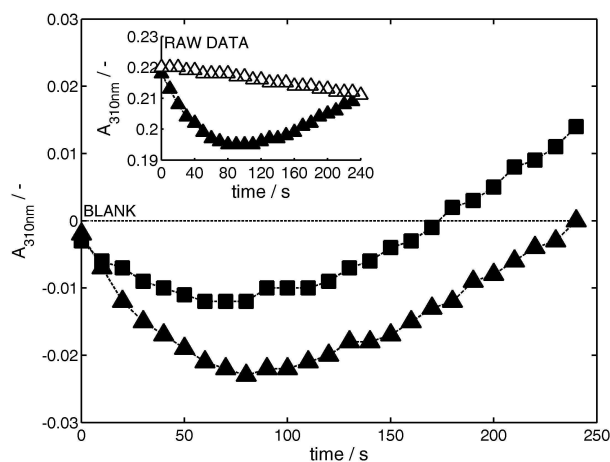


**Fig. 14.** Behavior of the spectrometric measurements (data are already corrected by blank) at an apparent H<sub>2</sub>O<sub>2</sub> overload. The adlerol (100 μM) to H<sub>2</sub>O<sub>2</sub> (100 μM (■) and 150 μM (▲)) ratio was 1 and 0.7, respectively. The inset plot shows the raw data (full assay (▲), VP-adlerol blank (△)) of absorption measurements at 310 nm for the initial adlerol to H<sub>2</sub>O<sub>2</sub> ratio of 1.

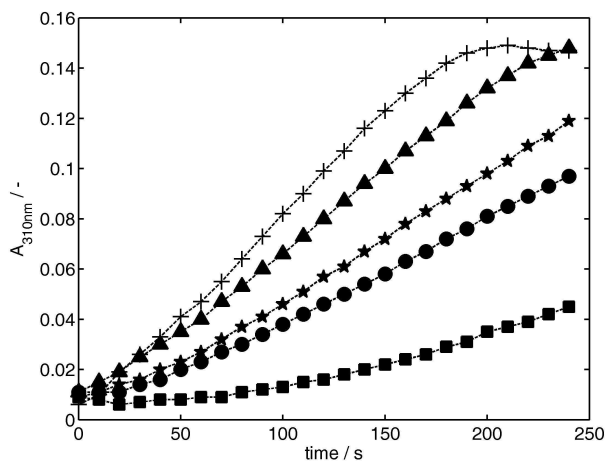


**Fig. 13.** Lag phase characteristic depending on the adlerol amount (100 μM (■), 250 μM (●), 500 μM (★), 750 μM (▲), and 1500 μM (+)) at a fixed initial H<sub>2</sub>O<sub>2</sub> concentration of 100 μM. The corresponding adlerol to H<sub>2</sub>O<sub>2</sub> ratios are 1, 2.5, 5, 7.5, and 15. Absorption values (data are already corrected by blank) at a wavelength of 310 nm are plotted as a function of measuring time.

Such events occurred at adlerol to H<sub>2</sub>O<sub>2</sub> ratios ranging from 1.3 (100 μM adlerol and 75 μM H<sub>2</sub>O<sub>2</sub>) up to 3.3 (500 μM adlerol and 150 μM H<sub>2</sub>O<sub>2</sub>) as long as the adlerol concentration will be maintained at ≤ 500 μM. At concentrations ≥ 750 μM the lag phase could still be monitored. Thus, concerning a fixed initial H<sub>2</sub>O<sub>2</sub> concentration (e.g. 100 μM (Fig. 13)), the duration of the lag period was reduced by elevating the adlerol content. Moreover, the reaction rate rose with adlerol as well.

#### 4.5. Spectral Soret Band Monitoring for Reaction Mechanism Interpretation

In order to clarify the events of several reactions seen above, the soret band behavior was again independently investigated under the same reaction conditions as executed for the kinetic measurements, except that just a fixed adlerol concentration of 1 mM was used. The corresponding results are graphically shown in Fig. 15; the characteristic wavelengths were already listed in Table 1. At λ = 310 nm in Fig. 15, an additional grey line is drawn to follow the VALd accumulation over time, simultaneously. The reaction mixture was monitored by a series of spectroscopic scans (wavelength area between

300 nm and 500 nm, with a step size of 2 nm) made every two minutes over a time period of  $t = 12$  min (inclusive pre-incubation phase of 7 min) starting from  $t = 0$  min. The last scan of pre-incubation was performed at  $t = 6$  min (blue solid line in **Fig. 15**, all previous scans are omitted). At the time  $t = 7$  min the reaction was initiated by  $H_2O_2$  addition. The first scan was made one minute later at  $t = 8$  min (red solid line in **Fig. 15**).

An additional reaction was conducted at  $350 \mu M H_2O_2$  to simulate a theoretical  $H_2O_2$  overload as reference (**Fig. 15F**). In such circumstances, preliminary studies using ABTS as reducing substrate showed some degree of inactivation of the used VP (data are not published). Indeed, monitoring VALd, similar results (initial drop in absorption) were received as seen in **Fig. 14**. Thus, enzyme deactivation may be expected.

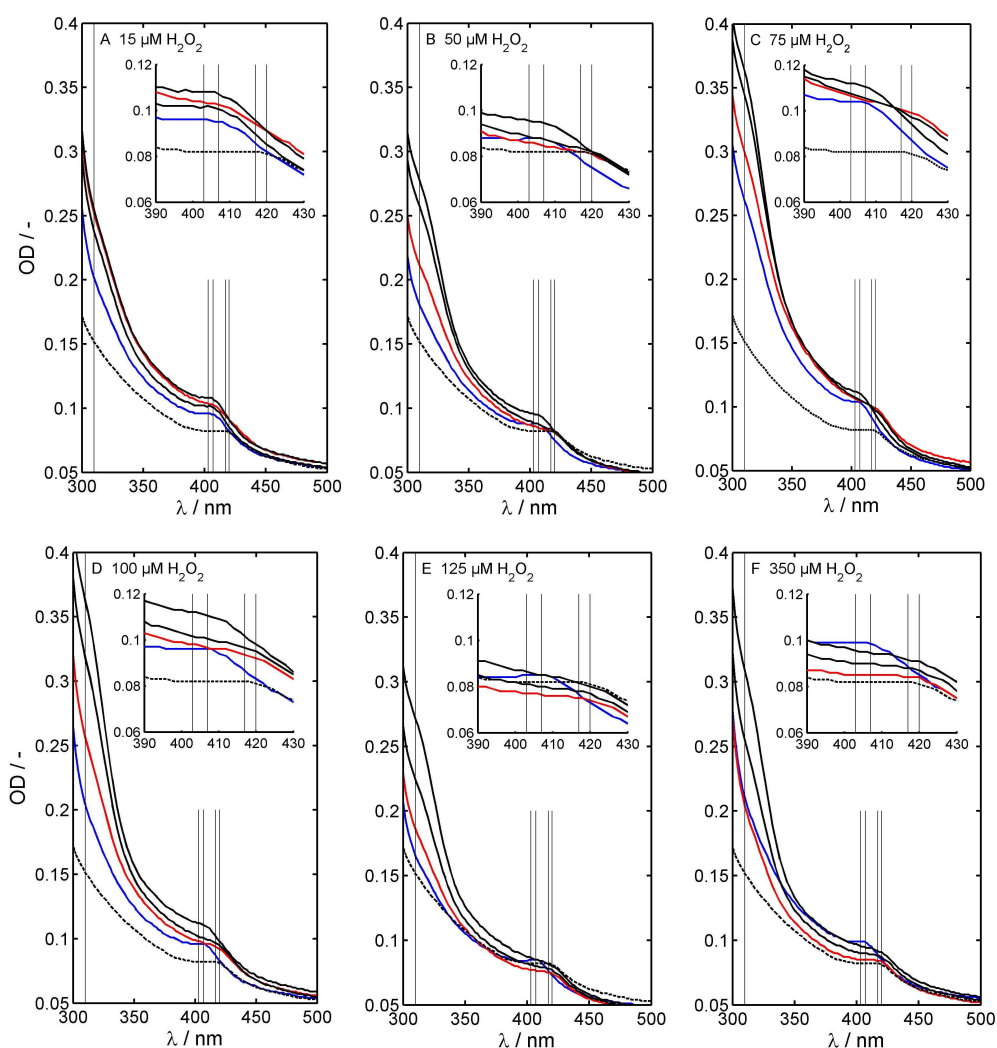


**Fig. 15.** Monitoring (raw data) of the soret band behavior (scan interval: 2 minutes, step size: 2 nm) after reaction start by adding A:  $15 \mu M$ , B:  $50 \mu M$ , C:  $75 \mu M$ , D:  $100 \mu M$ , E:  $125 \mu M$ , and F:  $350 \mu M H_2O_2$  at constant adlerol concentration of  $1 \text{ mM}$ . The blue solid line represents  $t = 6$  minutes of pre-incubation while the red solid line is the record of the first minute (or at  $t = 8$  minutes; pre-incubation plus measurement time) after reaction start. The end of reaction ( $t = 12$  minutes) is indicated by the upper black solid line, except in A. Here, the lower black solid line depicts the reaction end. Inset plots are zooms of the soret region. The black dotted line acts as reference and shows a spectral scan of a VP sample just incubated in  $350 \mu M H_2O_2$ .

At an initial H<sub>2</sub>O<sub>2</sub> concentration range of 50 μM to 100 μM H<sub>2</sub>O<sub>2</sub> depletion is assumed within ca. three minutes, based on the kinetic measurements above (therefore t = 10 min is supposed to be the last scan of reaction), whereas at 15 μM H<sub>2</sub>O<sub>2</sub> the reaction was already done after 1.5 min at the latest (the scan at t = 8 min (red solid line) should only be counted).

In **Fig. 15B-F** it can be extracted that after H<sub>2</sub>O<sub>2</sub> addition the soret band (407 nm) experienced a red shift to ca. 420 nm, similar to the spectral scan of a VP sample which was only be incubated in 350 μM H<sub>2</sub>O<sub>2</sub>. That would imply the VP reaction cycle passed through E<sup>III</sup> before return to E<sup>0</sup>. Furthermore, the soret band recovered by the end of reaction (around about H<sub>2</sub>O<sub>2</sub> depletion) at H<sub>2</sub>O<sub>2</sub> concentrations ≤ 100 μM, while E<sup>III</sup> remained unchanged above 100 μM H<sub>2</sub>O<sub>2</sub> (no H<sub>2</sub>O<sub>2</sub> depletion within the reaction period). Beside the red shift (blue solid line vs. red solid line), a considerable decrease in absorption intensity is seen in **Fig. 15E-F**, once H<sub>2</sub>O<sub>2</sub> exceeded 100 μM, which is probably associated with an enzyme inactivation process.

Although, the reaction was almost expired after the first spectrum was recorded in **Fig. 15A**, the cycle is assumed to follow the normal POX mechanism (**Fig. 1**) under such low H<sub>2</sub>O<sub>2</sub> conditions. However, a drop of the soret peak could also be registered at the end of examined period. By reconsidering **Fig. 14** (inset plot) in the preceding section in this context, a relative slow but constant decrease in absorption is noticed monitoring the VP-adlerol blank. This phenomenon, which was already mentioned throughout pre-incubation, appeared independently of the Adlerol amount in all studies with rates of ≤ 0.002 min<sup>-1</sup>. The same kind of behavior showed the full reaction assay after achieving H<sub>2</sub>O<sub>2</sub> depletion. At this point, evidence is taken that the major cause of any observed absorption decay is related to VP instabilities. Instability becomes more significant at low initial H<sub>2</sub>O<sub>2</sub> concentrations as well as lowered Adlerol content (**Fig. 15A** and to some degree in **Fig. 12 and 13** of the previous sub-chapter). VP inactivation and stability studies will be continued in the next section.

### 3.6. VP Inactivation/Deactivation by H<sub>2</sub>O<sub>2</sub> and the Impact of Adlerol

The influence of H<sub>2</sub>O<sub>2</sub> concentration on the VP stability was investigated as well as the impact of Adlerol. For this purpose, two series of experiments were carried out in a 10-50 mL scale by varying the initial

H<sub>2</sub>O<sub>2</sub> concentration (range: 0-1 mM) at initial Adlerol concentrations of 0 mM and 4 mM. The mixtures were continuously stirred with a stirrer speed of ca. 375 rpm. Enzyme stability was determined every three minutes (by ABTS assay) over a time period of 18 min. The observed deactivation constant k<sub>d(ops)</sub> was calculated by Equation (27) assuming enzyme deactivation follows first-order kinetics of the general formula given in Equation (22).



E indicates the active enzyme and E<sub>i</sub> the inactivated form. Since enzyme inactivation trended to incompleteness due to an expected H<sub>2</sub>O<sub>2</sub> consumption the enzyme concentration was modified and Equation (22) becomes to Equation (23).

$$\frac{d[E]}{dt} = k_{d(ops)} [E - E_\infty] \tag{23}$$

$$E_\infty = E \text{ at } t = \infty \tag{24}$$

$$[E_0] = [E] + [E_\infty] \tag{25}$$

Separation of the variables and integration for the boundary conditions

$$E_0 = E \text{ at } t = 0 \tag{26}$$

yields Equation (27).

$$-k_{d(ops)} = \frac{\ln\left(\frac{[E] - [E_\infty]}{[E_0] - [E_\infty]}\right)}{t} \tag{27}$$

In order to receive estimates of the enzyme half-life (t<sub>1/2</sub>) setting:

$$([E_0] - [E_\infty]) = 2([E] - [E_\infty]) \tag{28}$$

and

$$t = t_{1/2} \tag{29}$$

After substitution in Equation (27), a subsequent rearrangement to  $t_{1/2}$  yields Equation (30).

$$t_{1/2} = \frac{\ln(2)}{k_{d(\text{obs})}} \quad (30)$$

Based on Equation (27),  $k_{d(\text{obs})}$  was obtained from negative slopes of the straight lines generated by plotting the numerator against the denominator  $t$  (primary plots). Secondary plots of  $k_{d(\text{obs})}$  as a function of  $\text{H}_2\text{O}_2$  concentration in **Fig. 16** show a hyperbola dependence. The double-reciprocal plot in **Fig. 17** of the same data yields a linear relationship with non-zero intercept. According to Copeland (2000), the VP inactivation is subjected to a two-step mechanism with an initial binding step followed by a slower inactivation procedure (e.g. see combination of pathway 10, 11 and 12 in **Fig. 3**). The scheme is also known as time-dependent irreversible inhibition (Copeland, 2000; Marangoni, 2003). Therefore,  $k_{d(\text{obs})}$  was described through Equation (31) in the absence of adlerol. An impact of agitation on enzyme stability could be excluded for  $n \leq 600$  rpm (unpublished data).

$$k_{d(\text{obs})} = \frac{k_i^{\text{app}} [S_1]}{K_i^{\text{app}} + [S_1]} \quad (31)$$

where,  $S_1$  stands again for  $\text{H}_2\text{O}_2$ .

The parameter  $k_i^{\text{app}}$  represents the apparent maximal rate of enzyme inactivation, while  $K_i^{\text{app}}$  denotes the apparent concentration of inhibitor for reaching half-maximal rate of inactivation (Copeland, 2000). Both were obtained through the same non-linear curve fit approach as previously done for the steady-state kinetics, but using Equation (31). In order to solve the non-linear problem via the 'lsqcurvefit' function in MATLAB<sup>®</sup>, initial starting points for  $k_i^{\text{app}}$  and  $K_i^{\text{app}}$  were received from the intercept ( $b = 1/k_i^{\text{app}}$ ) and the slope ( $m = K_i^{\text{app}}/k_i^{\text{app}}$ ), respectively, of the linear regression (red solid line with the general formula  $y = mx + b$ ,  $x = c(\text{H}_2\text{O}_2)$  and  $y = k_{d(\text{obs})}$ ) made in **Fig. 17**. The results are listed in **Table 5**. In the presence of adlerol  $K_i^{\text{app}}$  increased, while  $k_i^{\text{app}}$  remained almost constant round about  $0.3 \text{ min}^{-1}$  comparing the red solid line (0 mM adlerol) with the black one (4 mM adlerol) in **Fig. 16 and 17**. Consequently, the inactivation mechanism was

competitive inhibited by adlerol (denoted as  $S_2$ ) which could be expressed via Equation (32). This equation also allows a first estimation of the adlerol dissociation constant  $K_m^{S_2}$ . For this purpose, the adlerol concentration was again considered to be constant. Initial values for  $k_i^{\text{app}}$  and  $K_i^{\text{app}}$  were transferred from previous calculations (Equation (31)). For  $K_m^{S_2}$  0.417 mM was specified initially based on the results in the sections above. Finally, the kinetic parameters were adjusted by non-linear curve fitting of both data sets (with and without adlerol) offering a reevaluation of  $k_i^{\text{app}}$  and  $K_i^{\text{app}}$  simultaneously. The data are also stored in **Table 5**.

$$k_{d(\text{obs})} = \frac{k_i^{\text{app}} [S_1]}{K_i^{\text{app}} \left( 1 + \frac{[S_2]}{K_m^{S_2}} \right) + [S_1]} \quad (32)$$

The ratio  $k_i^{\text{app}}/K_i^{\text{app}}$  reflects a second-order rate constant and is a measure of the inhibitory potency of an irreversible inhibitor (Copeland, 2000), such as  $\text{H}_2\text{O}_2$  in this case. The obtained value was  $25 \text{ M}^{-1} \text{ s}^{-1}$ .

Due to the inactivation characteristics in the presence of adlerol, **Fig. 16** can be clearly extracted that adlerol improved enzyme stability, in general. However, the half-life (inset plot of **Fig. 16**) decreased relative fast by an elevation of  $\text{H}_2\text{O}_2$  up to 100  $\mu\text{M}$  and strongly slowed down immediately afterwards.

## 5. DISCUSSION

The optimal pH of the VP being examined for the Mn-independent adlerol degradation was 3.5-4.0. With the same VP, but subsequently purified, an activity maximum at pH 3.0 (50 mM sodium tartrate buffer; 20°C) was recorded for VA conversion (Liers *et al.*, 2010). Based on **Table 6**, the pH optimum of ligninolytic enzymes (VP, LiP) varies between 3.0 and 4.0. In case of a polycyclic aromatic substrate a Mn-independent pH optimum was found at 4.0 (Wang *et al.*, 2003). In previous studies (data are still unpublished), pH values of  $\leq 3.5$  (50 mM sodium tartrate buffer) showed a higher impact on enzyme stability than temperature changes within 25-30°C. Moreover, the pH optimum for lignin degradation by ligninolytic cultures from *P. chrysosporium* is 4.5 (Schoemaker, 1990).

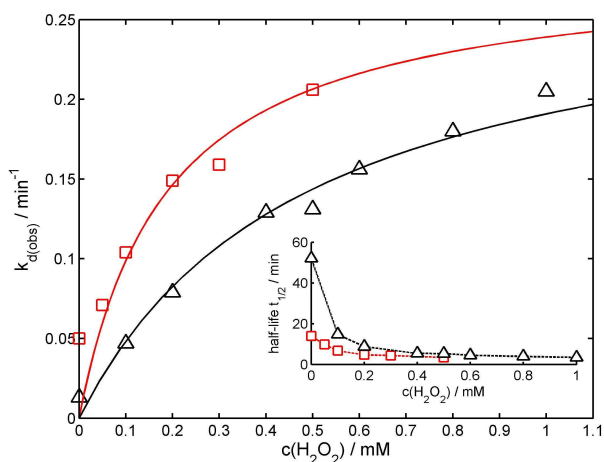


**Fig. 16.** H<sub>2</sub>O<sub>2</sub>-dependent deactivation kinetics in the absence of the substrate adlerol (experimental data (squares), computer simulation (red solid line)) and in the presence of 4 mM adlerol (experimental data (triangles), computer simulation (black solid line)). Reaction conditions: T: 30 ± 1°C, pH 4.0 (100 mM sodium tartrate buffer), n: 375 rpm, enzyme concentration: ca. 0.06 mg mL<sup>-1</sup>, V: 10 mL or 50 mL. Each examination was carried out in duplicates (parallel) with a maximal standard deviation of 10% from the mean. The inset plot illustrates the corresponding half-life (t<sub>1/2</sub>) course as a function of initial H<sub>2</sub>O<sub>2</sub> concentration.

Despite the fact, the used high concentrated buffer system seemed to slightly interfere the soret peak morphology, it was not possible to distinguish between E<sup>II</sup> and E<sup>III</sup>, since differentiation is difficult anyway (maxima are close together as seen in **Table 1**). Thus, a comparison was made with references, for instance, where VP was stored in distilled water only (reference for E<sup>0</sup>) or just in H<sub>2</sub>O<sub>2</sub> (reference for E<sup>III</sup> formation).

Indeed, conformational changes (kind of a burst phase, **Fig. 5**) could be recognized throughout enzyme pre-incubation with adlerol. For some reason, it was found that the VP was in its oxyform E<sup>III</sup> before it was brought up to its ground ferric state E<sup>0</sup>. This process was strongly affected by adlerol concentration (**Fig. 5**). Consequently, the question arises if this phenomenon is related to binary enzyme-substrate (ES) complex formation and stabilization processes, or does E<sup>III</sup> convert adlerol. There are no official statements regarding complex formation of ligninolytic POX with aromatic substrates as well as analogue by today, since the enzyme is not designed for direct contact with its centred heme group (Ruiz-Dueñas *et al.*, 2009a).

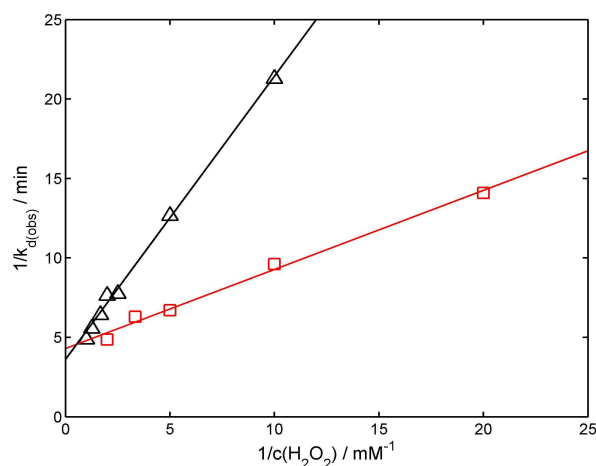


**Fig. 17.** Double-reciprocal plot of the data seen in **Fig. 16** as useful tool to distinguish 1-step (intercept will go through the origin) and 2-step (non-zero intercept) inactivation mechanism (according to Copeland (2002)). The solid lines are results of linear regression (y(x) = mx + b).

**Table 5.** Determined inactivation constants k<sub>i</sub><sup>app</sup>, and K<sub>i</sub><sup>app</sup> with simultaneous K<sub>m</sub><sup>S2</sup> estimation.

c(adlerol) μM	Kinetic constants			
	k <sub>i</sub> <sup>app</sup> min <sup>-1</sup>	K <sub>i</sub> <sup>app</sup> μM	k <sub>i</sub> <sup>app</sup> /K <sub>i</sub> <sup>app</sup> M <sup>-1</sup> s <sup>-1</sup>	K <sub>m</sub> <sup>S2</sup> μM
0	0.25	145	28.7 <sup>1)</sup>	n.a. <sup>2)</sup>
4000	0.28	188	24.8 <sup>1)</sup>	2,506

The kinetic constants represent the results of a non-linear curve fit using the mean observed deactivation constant k<sub>d(obs)</sub> of two measurements.

<sup>1)</sup> “best measure for inhibitory potency for an irreversible inhibitor is the second-order rate constant obtained from the ratio k<sub>i</sub><sup>app</sup>/K<sub>i</sub><sup>app</sup>” (Copeland, 2002)

<sup>2)</sup> not applicable

Contrary, an ABTS conversion study by HRP indicated a ter bi ping-pong mechanism (Cleland, 1963) with one ternary complex formation (E-H<sub>2</sub>O<sub>2</sub>-ABTS, while E-H<sub>2</sub>O<sub>2</sub> was defined as E<sup>I</sup>) prior HRP was transferred to its transition state E<sup>II</sup> and first product release occurred (Child and Bradslley, 1975).

In general, H<sub>2</sub>O<sub>2</sub> and reducing substrate do not bind on the same “active site” of the enzyme. Two separate access channels are identified in the literature. The first one is conserved in all POX and quasi reserved for H<sub>2</sub>O<sub>2</sub>

(direct contact to the enzyme's heme group), the second serves for reducing substrate (Ruiz-Dueñas *et al.*, 2009a). Due to the design of the second channel the enzyme substrate contact takes place at the enzyme's surface via a tryptophan component (in case of VP from *B. adusta*) which is supposed to be responsible for substrate oxidation, in its radical form (Pogni *et al.*, 2005; Ruiz-Dueñas *et al.*, 2009a).

However, based on the experimental data a conversion of adlerol by  $E^{III}$  would automatically imply the inability of  $E^0$  to degrade such a lignin model dimer as it is displayed through pathway 15 in **Fig. 3**.

A possible  $E^I$  formation due to reaction of  $E^{III}$  with adlerol (see also pathway 8 in **Fig. 3**) causing the said enzyme transformation could not be determined accurately (**Fig. 6**). Even it would be true, further conversion resulting in product (VAld) accumulation is expected as consequence, provided that  $E^I$  will be the defined active intermediate. Since it was found that adlerol was not further decomposed to VAld and saturation appeared, this theory is more unlikely.

VP kinetics could be sufficiently described by the well-known Michealis-Menten equation. Both,  $H_2O_2$  and adlerol had promotional effects on reaction velocity  $v$  in general. Nevertheless, pre-steady-state transients were recognized characterized by a  $H_2O_2$ -dependent lag phase in the time course of VAld accumulation. Usually, transient states are more expected to be fast (ms time scale) and may just be detectable throughout rapid-reaction techniques (Eisenthal and Danson, 2002). Indeed, the said lag phase was slow enough for sensing and appeared at  $H_2O_2$  concentrations  $\geq 50 \mu M$  under current reaction conditions. On the basis of the red shift of the soret band (**Fig. 15**), it will be presumed that the main cause of this phenomenon must have been an accumulation of  $E^{III}$  via  $E^{II}$  reaction with  $H_2O_2$ . Inhibitory effects of the co-substrate  $H_2O_2$  in such a way are known to slow down the reaction (Cai and Tien, 1992; Nicell *et al.*, 1993; Vlasits *et al.*, 2010).

Goodwin *et al.* (1994) obtained similar results studying the LiP catalyzed oxygen consumption with VA, and in presence of EDTA and oxalate as well. The  $O_2$  reduction rate appeared linear at low  $H_2O_2$  concentration of  $30 \mu M$ , whereas at values within the range of  $90 \mu M$  and  $120 \mu M$  lag phases could be noticed for the same reason ( $E^{III}$  formation).

If  $E^{III}$  can be transferred back to  $E^0$  was reviewed by pre-incubating the VP in  $H_2O_2$  ( $E^{III}$  formation was expected), under the known conditions, followed by adlerol addition for initiating the reaction. After a lag phase VAld production gradually restarted (**Fig. 18**) most likely due to  $E^{III}$  disappearance. It is conceivable that several enzyme molecules were still active (since no response in absorption signal could be detected after complete enzyme inactivation) to decompose adlerol along with certain products which served as substrate for  $E^{III}$ . This requires  $H_2O_2$  availability, though only in small amounts. The theory is based on studies examining the conversion of  $E^{III}$  of a LiP (LiP- $E^{III}$ ) from *P. chrysosporium* and VA besides 1,2,4,5-tetra-methoxybenzene as substrates (Barr and Aust, 1994). The researcher have been shown LiP- $E^{III}$  disappearance due to reaction with cation radical products to LiP- $E^0$  resulting in a reaction rate increase with time. If  $E^{III}$  of the used VP will be reactivated by an adlerol cation radical or a veratryl alcohol radical ( $VA^{\bullet}$ ) is questionable. It is proven that LiP- $E^{III}$  conversion to LiP- $E^0$  cannot occur via reaction with  $VA^{\bullet}$ , but with a veratryl alcohol cation radical ( $VA^{+\bullet}$ ) (Cai and Tien, 1992; Chung and Aust, 1995).

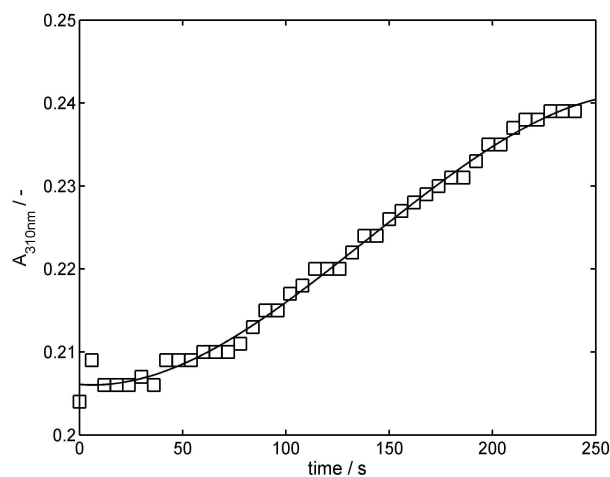


**Fig. 18.** Raw data for a reaction start by adlerol addition after seven minutes pre-incubation of VP with  $H_2O_2$  ( $300 \mu M$  considering the incomplete assay mixture) and  $E^{III}$  formation was expected. The usual reaction conditions were met with a final adlerol concentration of  $1 \text{ mM}$  and an enzyme amount of round about  $0.3 \text{ mg mL}^{-1}$  (in the full assay mixture). The black solid line is drawn just for orientation.

Furthermore,  $VA^{\bullet}$  is supposed to rapidly react with  $O_2$  to VAld under aerobic conditions (Schoemaker *et al.*, 1994b). Since the kinetics were conducted in  $O_2$  atmosphere,  $VA^{\bullet}$  as reductant for  $E^{III}$  can be excluded. Aerobic conditions may be further promoted due to  $O_2$  generation as a result of  $E^{III}$  formation (Nakajima and Yamazaki, 1987; Goodwin *et al.*, 1994). On the other hand, cation radical products are also limited in their lifetime. For  $VA^{+\bullet}$  a half-life of 40 ms was recorded (Harvey *et al.*, 1993). Finally, the radical decay is dependent on the nature of its substitutes (e.g.  $OCH_3$  (OMe) groups in **Fig. 2** favor formation and stabilization) (Wong, 2009). A conversion of  $E^{III}$  back to  $E^0$  by oxidation of an adlerol cation radical would imply less VAld accumulation, since one adlerol molecule will be only consumed throughout one reaction cycle. At least as long as the reaction passes the  $E^{III}$  intermediate. Thus, the reaction with adlerol has to be reconsidered at this point. At the end of the pre-incubation period with  $H_2O_2$ ,  $E^{III}$  is the predominant intermediate (supported by soret band behavior and by Barr and Aust (1994)) and a certain portion of enzyme is merely reversibly inhibited. That means,  $E^{III}$  may be the only reactant for adlerol. For evidence, further investigations have to be carried out.

When  $H_2O_2$  concentration was additionally increased and exceeded a certain limit (depending on the available adlerol content) noticeable rapid drop in the absorption signal was the consequence (**Fig. 14 and 15E-F**). Such  $H_2O_2$  concentrations were obviously sufficient to cause some degree of irreversible enzyme deactivation. Due to the fact that  $H_2O_2$  will be consumed throughout the process the drop declined with time. Once acceptable catalytic conditions were restored, accumulation of VAld was again measurable. This could be an explanation for the gradual decline of the apparent  $K_m^{app}$  at  $H_2O_2$  values  $\geq 100 \mu M$  in **Fig. 11B**. Since  $H_2O_2$  degraded faster than adlerol (mechanism-based), the enzyme:adlerol: $H_2O_2$  ratio was probably modified in such a way that the reaction rate  $v$  remained almost constant as seen in **Fig. 7**. Nevertheless, enzyme deactivation cannot be fully excluded even in the presence of sufficient adlerol content as well as by recovering  $E^0$  at low  $H_2O_2$  concentrations as it was seen in **Fig. 15A-D**. Although the current deactivation studies have demonstrated protective properties of adlerol, the enzyme activity/stability still undergoes a considerable impact by  $H_2O_2$  concentrations up to  $100 \mu M$  at clearly increased adlerol amounts of  $4 \text{ mM}$  (**Fig. 16 and 17**). In

this context, Aitken and Irvine (1989) and Hu *et al.* (1993) investigated deactivation kinetics of a LiP (and a MnP) from *P. chrysosporium*. Both working groups concluded that the lag phases, caused by  $E^{III}$  formation, are additionally associated with enzyme deactivation via  $E^{III}$ . It was found that the drop in the restored soret peak was proportional to loss in enzyme activity (Hu *et al.*, 1993).

Based on the soret band behavior, deactivation of the crude VP also appeared mainly through compound  $E^{III}$ , which will be promoted by the used acidic pH. A quick check showed that  $E^{III}$  formation did not occur when the VP under study was stored in distilled water, instead of the known buffer system, spiked with the same  $H_2O_2$  amount. An enhanced susceptibility of a VP from *Pleurotus pulmonarius* for  $H_2O_2$  with decreasing pH was also confirmed by Böckle *et al.* (1999).

Liers *et al.* (2010) examined VP (*B. adusta*) stability under acidic conditions (50 mM sodium tartrate buffer, pH 2.5) at  $20^\circ C$ . 70% loss in activity was recorded after 1 h of incubation. In the current work a half-life time of 52 min was found in the presence of adlerol at  $30^\circ C$  and 15 min once  $0.1 \text{ mM}$   $H_2O_2$  (initial concentration) was added, while the stability was halved in the absence of adlerol. A half-life time of just 1.3 min has even been reported in presence of  $1 \text{ mM}$   $H_2O_2$  (no substrate;  $60 \text{ mM}$  phosphate buffer, pH 6.1) (Valderrama and Vazquez-Duhalt, 2005).

In this study, VP deactivation mechanism by  $H_2O_2$  represents a time-dependent irreversible inhibition and is competitively inhibited in the presence of adlerol. The deactivation kinetic could be described satisfactorily by the model in Equation (32) assuming constant adlerol conditions. From estimates of  $k_i^{app}$  and  $K_i^{app}$  an average second-order rate constant of ca.  $25 \text{ M}^{-1} \text{ s}^{-1}$  was calculated.  $16 \text{ M}^{-1} \text{ s}^{-1}$  (pH 3.0;  $23^\circ C$ ) were measured for the  $H_2O_2$ -dependent inactivation process via  $E^{III}$  of a LiP (Aitken and Irvine, 1989). Furthermore, an additional estimation for the dissociation constant  $K_m^{S2}$  of  $2,506 \mu M$  was obtained indicating high substrate affinity. In comparison to the steady-state kinetics a  $K_m^{S2}$  value of just  $417 \mu M$  (**Table 3**) was determined at constant adlerol conditions. On the basis of the argumentation above, the estimated  $K_m^{S2}$  and the apparent steady-state kinetic parameters may differ from the true values, since a portion of enzyme and  $H_2O_2$  was partly lost when linear reaction velocities could be determined. Thus, the initial planned concentrations were not fully met. In such circumstances, obtained reaction velocities are underestimated (Kulmacz, 1986).

As pointed out at the beginning, kinetic constants for adlerol are seldom in the literature; none were found for VP. Instead, sufficient data are available for the reducing substrate VA (just for orientation purposes) and also a few for LiP and adlerol conversion. In **Table 6** several results from literature are listed for VP ( $Mn^{2+}$ -independent) and LiP. As it can be seen,  $K_m$  values  $> 3,000 \mu M$  are quite conceivable for VPs, also in conjunction with VA, whereas those for LiP are considerable lower. According to Liers *et al.* (2010), VP

is less active toward non-phenolic lignin model compounds than LiP. In addition, the question was raised as whether for ligninolytic peroxidases a great substrate excess (e.g. 25 mM) has to be required in order to reach maximal reaction rates (German *et al.*, 2011).

Finally, based on the current observations, the crude VP reaction mechanism for adlerol degradation will be assumed as summarized in **Fig. 19** for the next investigations, such as developing a  $H_2O_2$  feeding strategy.

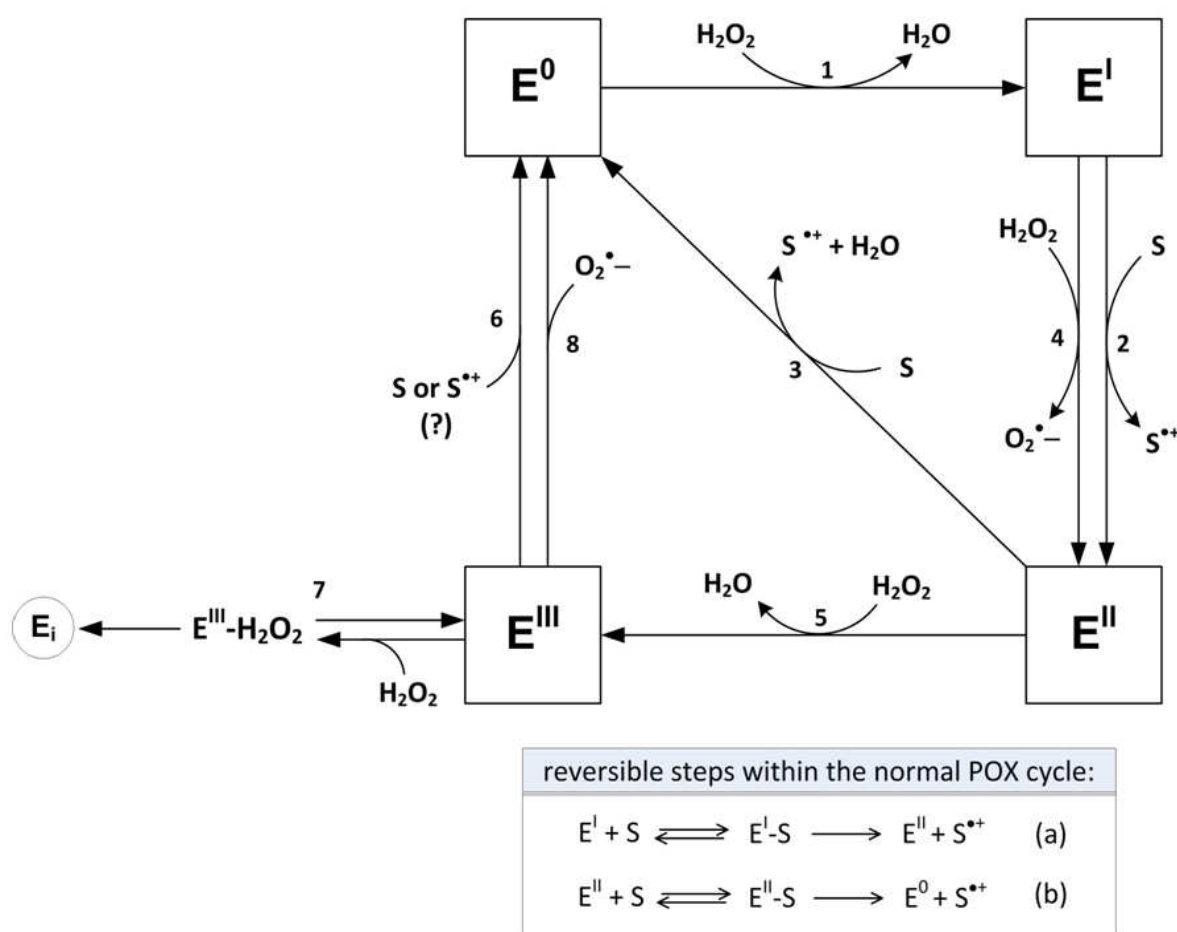


**Fig. 19.** Supposed  $H_2O_2$ -dependent reaction mechanism of the crude VP from *B. adusta* for adlerol degradation.  $E^0$ - $E^{III}$  are enzyme intermediates. The symbols  $S$  and  $S^{*+}$  stand for an appropriate substrate (e.g. adlerol) and its corresponding radical cation, respectively.  $O_2^{\bullet-}$  denotes superoxide radical anions. Pathway 1-3 depicts the usual POX reaction cycle with the reversible steps described by Equation (a) and (b) (Ruiz-Dueñas *et al.*, 2009b). The cycle will be initiated by  $H_2O_2$  (pathway 1). Pathway 4, 5, and 7 show important side reactions with  $H_2O_2$  which competes with pathway 6. Enzyme deactivation ( $E_i$ ; inactivated enzyme) is found to occur via  $E^{III}$  as sketched in pathway 7. Pathway 8 illustrates a spontaneous unimolecular decay of  $E^{III}$ .

**Table 6.** Compilation of some kinetic investigation results for H<sub>2</sub>O<sub>2</sub> and different monomeric and polymeric aromatic substrates.

Peroxidase	Substrate S	k <sub>cat</sub> s <sup>-1</sup>	v <sub>max</sub> μM min <sup>-1</sup>	K <sub>m</sub> <sup>S</sup> μM	Initial reaction conditions	Reference
VP ( <i>Bjerkandera adusta</i> )	H <sub>2</sub> O <sub>2</sub>	n.a.	n.a.	200	pH: 4.0 / T: 25°C / 50 mM malonate buffer / reducing substrate: PAH <sup>1)</sup>	Wang <i>et al.</i> , 2003
	PAH <sup>1)</sup>	2.4 <sup>2)</sup>	n.a.	23,800	0.1 mM H <sub>2</sub> O <sub>2</sub>	
VP ( <i>Bjerkandera species</i> )	H <sub>2</sub> O <sub>2</sub>	n.a.	28 (U mg <sup>-1</sup> )	182	pH: 3.0 / RT / 0.5 mM VA / ca. 0.1 mM sodium tartrate buffer	Moreira <i>et al.</i> , 2006
	VA	n.a.	13 (U mg <sup>-1</sup> )	1,500	pH: 3.0 / ca. 320 μM H <sub>2</sub> O <sub>2</sub>	
	VA	n.a.	83 (U mg <sup>-1</sup> )	3,670	pH: 5.0	
VP ( <i>Bjerkandera species</i> strain BOS55)	VA	1.4-2.8	7.6-15.6 <sup>3)</sup>	116-534	pH: 3.0 and 4.5 / 0.1 mM H <sub>2</sub> O <sub>2</sub> / 50 mM succinate buffer / [E]: 4 mg L <sup>-1</sup>	Mester and Field, 1998
VP ( <i>Pleurotus eryngii</i> )	H <sub>2</sub> O <sub>2</sub>	n.a.	n.a.	2-3	pH: 3.0 / 2 mM VA / 0.1 mM sodium tartrate buffer	Camarero <i>et al.</i> , 1999
	VA	n.a.	n.a.	3,500	pH: 3.0 / 0.4 mM H <sub>2</sub> O <sub>2</sub> / 0.1 mM sodium tartrate buffer	
	VA	n.a.	45-95 (U mg <sup>-1</sup> )	3,000-3,500	pH: 3.0 / 0.1 mM H <sub>2</sub> O <sub>2</sub> / 0.1 mM sodium tartrate buffer	Martínez <i>et al.</i> , 1996
LiP ( <i>Phlebia radiate</i> )	H <sub>2</sub> O <sub>2</sub>	3.7	8.9 <sup>4)</sup>	11	pH: 3.0 / T: 25°C / 1-50 μM H <sub>2</sub> O <sub>2</sub> / 1 mM VA / [E]: 40 nM	Lundell <i>et al.</i> , 1993b
	VA	7.1	17.0 <sup>4)</sup>	149	pH: 3.0 / T: 25°C / 0.2 mM H <sub>2</sub> O <sub>2</sub> / 2-500 μM VA / [E]: 40 nM	
	adlerol	4.7	11.3 <sup>4)</sup>	192	similar to VA above	
LiP ( <i>Phanerochaete</i> <i>chrysosporium</i> )	dimeric non- phenolic LMC <sup>5)</sup>	n.a.	n.a.	55	pH: 3.0 / T: 37°C / 0.2 mM H <sub>2</sub> O <sub>2</sub> / 0.1 mM sodium tartrate buffer / 0.1% Tween 80 / 5 μg mL <sup>-1</sup> protein	Tien and Kirk, 1984
LiP	β-O-4 (adlerol)	0.5	54 <sup>4)</sup>	160	pH: 3.5 / T: 25°C / 50 μM H <sub>2</sub> O <sub>2</sub> / 0.05-2.5 mM S / 125 mM tartrate / [E]: 1.8 μM	Cho <i>et al.</i> , 2010

<sup>1)</sup> PAH: polycyclic aromatic hydrocarbon,

<sup>2)</sup> original data was 145 min<sup>-1</sup>,

<sup>3)</sup> original data were 1.9-3.9 U mg<sup>-1</sup>,

<sup>4)</sup> subsequently calculated based on given data assuming v<sub>max</sub> = k<sub>cat</sub> [E],

<sup>5)</sup> 1,2-bis-(3-methoxy-4-methoxyphenyl)-propane-1,3-diol

It is suggested that the normal VP reaction cycle (without  $E^{III}$  formation) involves reversible reaction steps. Despite a further review regarding applicability of the kinetic models described through Equation (13) or (19) as well. An approval is given by Ruiz-Dueñas *et al.* (2009b) who investigated transient state kinetics of a recombinant native VP (obtained by *E. coli*) with the substrate VA (Equation (6)-(7)).  $E^I$  formation via two-electron oxidation of  $E^0$  by  $H_2O_2$  “has long been understood” (Dunford, 2010). Moreover, it will be supposed that  $E^{II}$  is directly reduced by adlerol (assumption is general accepted, e.g. for VA oxidation (Ruiz-Dueñas *et al.*, 2009b)). However, the evidence for this assumption is still pending.

Deactivation of the crude VP is supposed to occur as described by pathway 7 (Fig. 19). Nevertheless, activity loss via spontaneous unimolecular decay of  $E^I$  (is unstable (Dunford, 2010); is omitted in Fig. 19) and  $E^{III}$  to  $E^{II}$  and  $E^0$ , respectively, have to be taken into account for mathematical modeling and process simulation. The same probably applies for side reaction of  $E^I$  with  $H_2O_2$  to  $E^{II}$  (pathway 4, Fig. 19) or even directly to  $E^{III}$  (Vlasits *et al.*, 2010), in case  $H_2O_2$  exceeds a certain amount.

## 6. CONCLUSION

“Due to the complexity of the degradation reactions of  $\beta$ -O-4 compounds it is difficult to find solid experimental support” (Lundell *et al.*, 1993a). In addition, definite conclusions are generally hampered, since a crude enzyme was used. However, focusing bioprocess engineering, e.g. implementation of online monitoring systems along with developing feeding strategies, important insights could be gained into the reaction mechanism as follows.

The crude VP from *B. adusta* showed saturation kinetics (described by Michaelis-Menten equation) for adlerol degradation with relative sensitive response to  $H_2O_2$ . This was characterized by slow transient states in form of a lag phase most likely caused by  $E^{III}$  formation via  $E^{II}$  reaction with  $H_2O_2$  prior steady state. Furthermore,  $E^{III}$  could be (partly) converted back to  $E^0$  for restarting a catalytic cycle. Whether that was triggered by adlerol or its cation radical product still has to be verified.

The VP deactivation by  $H_2O_2$  followed a time-dependent irreversible mechanism and occurred mainly through  $E^{III}$ . Deactivation was diminished in presence of adlerol indicating protective properties of the substrate. Hence, evidence is taken that a competition

occurs between  $H_2O_2$  and adlerol or its radical cation products, respectively, for reactions with  $E^{II}$  as well as  $E^{III}$ .

Regardless the proven catalytic activity of  $E^{III}$ , it is recommended to maintain  $H_2O_2$  concentrations below 50  $\mu$ M at an adlerol to  $H_2O_2$  ratio of at least 15:1 in order to minimize enzyme reactions as well as enzyme losses via  $E^{III}$ . From the bioprocess engineering point of view, this implies relative slow  $H_2O_2$  feeding rates, or in other words, a fine tuning of  $H_2O_2$  concentration concerning fed-batch and continuous operational modes in bioreactors. Indeed, low *in vitro*  $H_2O_2$  concentrations are assumed (Hammel *et al.*, 1993; Böckle *et al.*, 1999), since  $H_2O_2$  is obviously assimilated by the fungal mycelium avoiding unfavorable high concentrations *in vivo* (Böckle *et al.*, 1999). In addition, the reducing substrate amount and the enzyme needs to be balanced as well.

## 7. ACKNOWLEDGEMENT

The researchers would like to thank the Hessen State Ministry of Higher Education, Research and the Arts for the financial support within the Hessen initiative for scientific and economic excellence (LOEWE).

## 8. REFERENCES

- Acosta, M., J.A. del Río, M.B. Arnao, J. Sánchez-Bravo and F. Sabater *et al.*, 1988. Oxygen consumption and enzyme inactivation in the indolyl-3-acetic acid oxidation catalyzed by peroxidase. *Biochimica et Biophysica Acta (BBA)-Protein Structure Mol. Enzymol.*, 955: 194-202. DOI: 10.1016/0167-4838(88)90193-8
- Adler, E., 1977. Lignin chemistry-past, present and future. *Wood Sci. Technol.*, 11: 169-218. DOI: 10.1007/BF00365615
- Aitken, M.D. and R.L. Irvine, 1989. Stability testing of ligninase and Mn-peroxidase from *Phanerochaete chrysosporium*. *Biotechnol. Bioeng.*, 34: 1251-1260. DOI: 10.1002/bit.260341003
- Andrawis, A., K.A. Johnson and M. Tien, 1988. Studies on compound I formation of the lignin peroxidase from *Phanerochaete chrysosporium*. *J. Biol. Chem.*, 263: 1195-1198. PMID: 3335539
- Arnao, M.B., M. Acosta, J.A. del Río and F. García-Cánovas, 1990a. Inactivation of peroxidase by hydrogen peroxide and its protection by a reductant agent. *Biochim. Biophys. Acta (BBA)-Protein Struct. Mol. Enzymol.*, 1038: 85-89. DOI: 10.1016/0167-4838(90)90014-7

- Arnao, M.B., M. Acosta, J.A. del Río, R. Varón and F. García-Cánovas, 1990b. A kinetic study on the suicide inactivation of peroxidase by hydrogen peroxide. *Biochim. Biophys. Acta (BBA)-Protein Struct. Mol. Enzymol.*, 1041: 43-47. DOI: 10.1016/0167-4838(90)90120-5
- Bakovic, M. and H.B. Dunford, 1993. Kinetics of the oxidation of p-coumaric acid by prostaglandin H synthase and hydrogen peroxide. *Biochemistry*, 32: 833-840. DOI: 10.1021/bi00054a014
- Barr, D.P. and S.D. Aust, 1994. Conversion of lignin peroxidase compound III to active enzyme by cation radicals. *Arch. Biochem. Biophys.*, 312: 511-515. DOI:10.1006/abbi.1994.1339
- Bielski, B.H., D.E. Cabelli, L.A. Ravindra and A.B. Ross, 1985. Reactivity of HO<sub>2</sub>/O<sub>2</sub>- Radicals in aqueous solution. *J. Phys. Chem. Ref. Data*, 14: 1041-1100.
- Bisswanger, H., 2008. *Enzyme Kinetics: Section 2*. In: *Enzyme Kinetics*, (Eds.), Wiley-VCH Verlag GmbH and Co. KGaA, ISBN-10: 9783527319572, pp: 124-193.
- Böckle, B., M.J. Martínez, F. Guillén and Á.T. Martínez, 1999. Mechanism of peroxidase inactivation in liquid cultures of the ligninolytic fungus *Pleurotus pulmonarius*. *Applied Environ. Microbiol.*, 65: 923-928. PMID: PMC91124
- Cai, D. and M. Tien, 1992. Kinetic studies on the formation and decomposition of compounds II and III. Reactions of lignin peroxidase with H<sub>2</sub>O<sub>2</sub>. *J. Biol. Chem.*, 267: 11149-11155. PMID: 1317857
- Camarero, S., S. Sarkar, F.J. Ruiz-Dueñas, M.J. Martínez and Á.T. Martínez, 1999. Description of a versatile peroxidase involved in the natural degradation of lignin that has both manganese peroxidase and lignin peroxidase substrate interaction sites. *J. Biol. Chem.*, 274: 10324-10330. DOI: 10.1074/jbc.274.15.10324
- Chance, B. and A.C. Maehly, 1955. [136] Assay of Catalases and Peroxidases. 1st Edn., *Methods in Enzymology*, Academic Press, pp: 764-775.
- Child, R.E. and W.G. Bradsley, 1975. The steady-state kinetics of peroxidase with 2,2'-azino-di-(3-ethylbenzthiazoline-6-sulphonic acid) as chromogen. *Biochem. J.*, 145: 93-103. PMID: PMC1165190
- Cho, D.W., R. Parthasarathi, A.S. Pimentel, G.D. Maestas and H.J. Park *et al.*, 2010. Nature and kinetic analysis of carbon-carbon bond fragmentation reactions of cation radicals derived from SETOxidation of lignin model compounds. *J. Organic Chem.*, 75: 6549-6562.
- Chung, N. and S.D. Aust, 1995. Inactivation of lignin peroxidase by hydrogen peroxide during the oxidation of phenols. *Arch. Biochem. Biophys.*, 316: 851-855. DOI: 10.1006/abbi.1995.1114
- Cleland, W.W., 1963. The kinetics of enzyme-catalyzed reactions with two or more substrates or products: I. Nomenclature and rate equations. *Biochim. Biophys. Acta (BBA)-Specialized Section Enzymological Subjects*, 67: 104-137. DOI: 10.1016/0926-6569(63)90211-6
- Copeland, D.C., 2000. *The Origins of Major War*. 1st Edn., Cornell University Press, Ithaca, ISBN-10: 0801437504, pp: 322.
- Cornish-Bowden, A., 2012. *Fundamentals of Enzyme Kinetics*. 1st Edn., Wiley-Blackwell, ISBN-10: 9783527330744, pp: 510.
- Dashtban, M., H. Schraft, T.A. Syed and W. Qin, 2010. Fungal biodegradation and enzymatic modification of lignin. *Int. J. Biochem. Mol. Biol.*, 1: 36-50. PMC: 3180040
- Dunford, H.B., 1991. Horseradish Peroxidase: Structure and Kinetic Properties. In: *Peroxidases in Chemistry and Biology*, Everse, J. (Ed.), CRC Press Inc., pp: 1-24.
- Dunford, H.B., 2010. *Peroxidases and Catalases: Biochemistry, Biophysics, Biotechnology and Physiology*. 1st Edn., John Wiley and Sons. ISBN-10: 9780470224762, pp: 459.
- Eisenthal, R. and M.J. Danson, 2002. *Enzyme Assays: A practical approach*, Oxford University Press, USA., ISBN-10: 0199638209, pp: 302.
- Ek, M., G. Gellerstedt and G. Henriksson, 2009. *Wood Chemistry and Wood Biotechnology (Pulp and Paper Chemistry and Technology)*, ISBN-10: 978-3-11-021340-9, pp: 308.
- Eriksson, K.E.L., R.A. Blanchette and P. Ander, 1990. *Microbial and enzymatic degradation of wood and wood components*, Springer-Verlag. pp: ix + 407
- García-Ruiz, E., D. Gonzalez-Perez, F.J. Ruiz-Dueñas, Á.T. Martínez and M. Alcalde, 2012. Directed evolution of a temperature-, peroxide- and alkaline pH-tolerant versatile peroxidase. *Biochem. J.*, 441: 487-498. DOI: 10.1042/bj20111199
- German, D.P., M.N. Weintraub, A.S. Grandy, C.L. Lauber and Z.L. Rinkes *et al.*, 2011. Optimization of hydrolytic and oxidative enzyme methods for ecosystem studies. *Soil Biol. Biochem.*, 43: 1387-1397. DOI: 10.1016/j.soilbio.2011.03.017
- Giardina, P., G. Palmieri, B. Fontanella, V. Riviello and G. Sannia, 2000. Manganese Peroxidase Isoenzymes Produced by *Pleurotus ostreatus* Grown on Wood Sawdust. *Archives of Biochemistry and Biophysics* 376: 171-179. DOI: 10.1006/abbi.1999.169

- Goodwin, D.C., D.P. Barr, S.D. Aust and T.A. Grover, 1994. The role of oxalate in lignin peroxidase-catalyzed reduction: Protection from compound iii accumulation. *Arch. Biochem. Biophys.*, 315: 267-272. DOI: 10.1006/abbi.1994.1499
- Halliwell, B. and J.M.C. Gutteridge, 1985. The importance of free radicals and catalytic metal ions in human diseases. *Mol. Aspects Med.*, 8: 89-193. DOI: 10.1016/0098-2997(85)90001-9
- Hammel, K.E., K.A. Jensen, M.D. Mozuch, L.L. Landucci and M. Tien *et al.*, 1993. Ligninolysis by a purified lignin peroxidase. *J. Biol. Chem.*, 268: 12274-12281. PMID: 8509364
- Harman, L.S., D.K. Carver, J. Schreiber and R.P. Mason, 1986. One- and two-electron oxidation of reduced glutathione by peroxidases. *J. Biol. Chem.*, 261: 1642-1648. PMID: 3020935
- Harvey, P.J., L.P. Candelas, D. Renzoni, P. Jones, P. Wardman and J.M. Palmer, 1993. Plant peroxidases: Biochemistry and physiology. Proceedings of the International Symposium of Plant Peroxidases III, Jul. 10-14, Elsinore, Denmark, University of Copenhagen and University of Geneva, pp: 185- 191.
- Hatakka, A., T. Lundell, A.L.M. Tervila-Wilo and G. Brunow, 1991. Metabolism of non-phenolic  $\beta$ -O-4 lignin model compounds by the white-rot fungus *Phlebia radiata*. *Applied Microbiol. Biotechnol.*, 36: 270-277. DOI: 10.1007/BF00164433
- Howard, R.L., E. Abotsi, E.L. Jansen van Rensburg and S. Howard, 2003. Lignocellulose biotechnology: Issues of bioconversion and enzyme production. *African J. Biotechnol.*, 2: 602-619.
- Hu, Z.C., R.A. Korus, C.R. Venkataramu and R.L. Crawford, 1993. Deactivation kinetics of lignin peroxidase from *Phanerochaete chrysosporium*. *Enzyme Microbiol. Technol.*, 15: 567-574. DOI: 10.1016/0141-0229(93)90018-W
- Jantschko, W., P.G. Furtmuller, M. Zederbauer, K. Neugschwandtner and C. Jakopitsch *et al.*, 2005. Reaction of ferrous lactoperoxidase with hydrogen peroxide and dioxygen: An anaerobic stopped-flow study. *Arch. Biochem. Biophys.*, 434: 51-59.
- Jena Bioscience, 2010. Data Sheet Versatile Peroxidase EC 1.11.1.16, Mn(II): H<sub>2</sub>O<sub>2</sub> oxidoreductase/diarylpropane: O<sub>2</sub>, H<sub>2</sub>O<sub>2</sub> oxidoreductase, Bjerkandera adusta.
- Kamm, B., M. Kamm, P.R. Gruber and S. Kromus, 2008. Biorefinery Systems-An Overview. 1st Edn., Biorefineries-Industrial Processes and Products, (Eds.), Wiley-VCH Verlag GmbH, pp: 1-40.
- Kanofsky, J.R., 1991. Peroxidase-Catalyzed Generation of Singlet Oxygen and of Free Radicals. In: Peroxidases in chemistry and biology. Everse, J., (Eds.), CRC Press Inc., pp: 219-237.
- Kettle, A.J., R.F. Anderson, M.B. Hampton and C.C. Winterbourn, 2007. Reactions of Superoxide with Myeloperoxidase *Biochem.*, 46: 4888-4897. DOI: 10.1021/bi602587k
- Kirk, T.K. and R.L. Farrell, 1987. Enzymatic combustion: The microbial degradation of lignin. *Annu. Rev. Microbiol.*, 41: 465-505. DOI: 10.1146/annurev.mi.41.100187.002341
- Kirk, T.K., M. Tien, P.J. Kersten, M.D. Mozuch and B. Kalyanaraman, 1986. Ligninase of *Phanerochaete chrysosporium*. Mechanism of its degradation of the non-phenolic arylglycerol  $\beta$ -aryl ether substructure of lignin. *Biochem. J.*, 236: 279-287. PMID: PMC1146817
- Kulmacz, R.J., 1986. Prostaglandin H synthase and hydroperoxides: Peroxidase reaction and inactivation kinetics. *Arch. Biochem. Biophys.*, 249: 273-285. DOI: 10.1016/0003-9861(86)90003-2
- Lange, J.P., 2007. Lignocellulose conversion: An introduction to chemistry, process and economics. *Biofuels, Bioproducts Biorefin.*, 1: 39-48. DOI: 10.1002/9783527621118.ch2
- Liers, C., C. Bobeth, M. Pecyna, R. Ullrich and M. Hofrichter, 2010. DyP-like peroxidases of the jelly fungus *Auricularia auricula-judae* oxidize nonphenolic lignin model compounds and highredox potential dyes. *Applied Microbiol. Biotechnol.*, 85: 1869-1879. DOI: 10.1007/s00253-009-2173-7
- Lundell, T., H. Schoemaker, A. Hatakka and G. Brunow, 1993a. New mechanism of the C $\alpha$ -C $\beta$  cleavage in non-phenolic arylglycerol  $\beta$ -aryl ether lignin substructures catalyzed by lignin peroxidase. *Holzforschung-Int. J. Biol. Chem. Phys. Technol. Wood*, 47: 219. DOI: 10.1515/hfsg.1993.47.3.219
- Lundell, T., R. Wever, R. Floris, P. Harvey and A. Hatakka *et al.*, 1993b. Lignin peroxidase L3 from *Phlebia radiata*. Pre-steadystate and steady-state studies with veratryl alcohol and a non-phenolic lignin model compound 1-(3,4-dimethoxyphenyl)-2-(2-methoxyphenoxy)propane-1,3-diol. *Eur. J. Biochem.*, 211: 391-402.
- Marangoni, A.G., 2003. Enzyme Kinetics: A Modern Approach. 1st Edn., Wiley-Interscience. ISBN-10: 0471461415, pp: 229.

- Martínez, A.T., 2007. High Redox Potential Peroxidases. 1st Edn., Industrial Enzymes. Polaina, J. and A. Mac- Cabe, (Eds.), Springer Netherlands, ISBN-10: 9781402053771, pp: 477-488.
- Martínez, A.T., M. Speranza, F.J. Ruiz-Dueñas, P. Ferreira and S. Camarero *et al.*, 2005. Biodegradation of lignocellulosics: Microbial, chemical and enzymatic aspects of the fungal attack of lignin. *Int. Microbiol.*, 8: 195-204. PMID: 16200498
- Martínez, M.J., F.J. Ruiz-Dueñas, F. Guillén and Á.T. Martínez, 1996. Purification and catalytic properties of two manganese peroxidase isoenzymes from *Pleurotus eryngii*. *Europ. J. Biochem.*, 237: 424-432. DOI:10.1111/j.1432-1033.1996.0424k.x
- Mester, T. and J.A. Field, 1998. Characterization of a Novel Manganese Peroxidase-Lignin Peroxidase Hybrid Isozyme Produced by Bjerkandera Species Strain BOS55 in the Absence of Manganese. *J. Biol. Chem.*, 273: 15412-15417. DOI: 10.1074/jbc.273.25.15412
- Moreira, P.R., F. Bouillenne, E. Almeida-Vara, F. Xavier Malcata, J.M. Frere and J.C. Duarte, 2006. Purification, kinetics and spectral characterisation of a new versatile peroxidase from a Bjerkandera sp. isolate. *Enzyme Microb. Technol.*, 38: 28-33. DOI: 10.1016/j.enzmictec.2004.12.035
- Nakajima, R. and I. Yamazaki, 1987. The mechanism of oxypoxidase formation from ferryl peroxidase and hydrogen peroxide. *J. Biol. Chem.*, 262: 2576-2581. PMID: 3029087
- Nakamura, M., I. Yamazaki, T. Kotani and S. Ohtaki, 1985. Thyroid peroxidase selects the mechanism of either 1- or 2- electron oxidation of phenols, depending on their substituents. *J. Biol. Chem.*, 260: 13546-13552. PMID: 2997169
- Nicell, J.A., J.K. Bewtra, N. Biswas and E. Taylor, 1993. Reactor development for peroxidase catalyzed polymerization and precipitation of phenols from wastewater. *Water Res.*, 27: 1629-1639. DOI: 10.1016/0043-1354(93)90127-4
- Palmer, J.M., P.J. Harvey and H.E. Schoemaker, 1987. The role of Peroxidases, Radical Cations and Oxygen in the degradation of Lignin [and Discussion]. *Phil. Trans. R. Soc. Lond. A* 321: 495-505. DOI: 10.1098/rsta.1987.0027
- Pérez-Boada, M., F.J. Ruiz-Duenas, R. Pogni, R. Basosi and T. Choinowski *et al.*, 2005. Versatile peroxidase oxidation of high redox potential aromatic compounds: Site-directed mutagenesis, spectroscopic and crystallographic investigation of three long-range electron transfer pathways. *J. Mol. Biol.*, 354: 385-402. DOI: 10.1016/j.jmb.2005.09.047
- Pogni, R., M.C. Baratto, S. Giansanti, C. Teutloff and J. Verdin *et al.*, 2005. Tryptophan-based radical in the catalytic mechanism of versatile peroxidase from *Bjerkandera adusta*. *Biochemistry*, 44: 4267-4274. DOI: 10.1021/bi0474741
- Promega, 2009. Calculating Nucleic Acid or Protein Concentration Using the GloMax® Multi+ Microplate Instrument. Last modified date July 07, 2009
- Rasmussen, C.B., H.B. Dunford and K.G. Welinder, 1995. Rate enhancement of compound i formation of barley peroxidase by ferulic acid, caffeic acid and coniferyl alcohol. *Biochemistry*, 34: 4022-4029. DOI: 10.1021/bi00012a021
- Ruiz-Dueñas, F.J., M. Morales, E. Garcia, Y. Miki and M.J. Martínez *et al.*, 2009a. Substrate oxidation sites in versatile peroxidase and other basidiomycete peroxidases. *J. Exp. Bot.*, 60: 441-452. DOI: 10.1093/jxb/ern261
- Ruiz-Dueñas, F.J., M.J. Martínez and Á.T. Martínez, 1999. Molecular characterization of a novel peroxidase isolated from the ligninolytic fungus *Pleurotus eryngii*. *Mol. Microbiol.*, 31: 223-235. DOI:10.1046/j.1365-2958.1999.01164.x
- Ruiz-Dueñas, F.J., R. Pogni, M. Morales, S. Giansanti and M.J. Mate *et al.*, 2009b. Protein radicals in fungal versatile peroxidase: Catalytic tryptophan radical in both compound i and compound ii and studies on W164Y, W164H and W164S Variants. *J. Biol. Chem.*, 284: 7986-7994. DOI: 10.1074/jbc.M808069200
- SAC, 2012. Enabling science to improve the quality of life. Sigma-Aldrich Co. LLC.
- Sánchez, C., 2009. Lignocellulosic residues: Biodegradation and bioconversion by fungi. *Biotechnol. Adv.*, 27: 185-194. DOI: 10.1016/j.biotechadv.2008.11.001
- Schoemaker, H.E. and K. Piontek, 1996. On the interaction of lignin peroxidase with lignin. *Pure Applied Chem.*, 8: 2089-2096. DOI: 10.1351/pac199668112089
- Schoemaker, H.E., 1990. On the chemistry of lignin biodegradation. *Recueil des Travaux Chimiques des Pays-Bas*, 109: 255-272. DOI: 10.1002/recl.19901090402
- Schoemaker, H.E., T.K. Lundell, A.I. Hatakka and K. Piontek, 1994b. The oxidation of veratryl alcohol, dimeric lignin models and lignin by lignin peroxidase: The redox cycle revisited. *FEMS Microbiol. Rev.*, 13: 321-331. DOI: 10.1111/j.1574-6976.1994.tb00052.x

- Schoemaker, H.E., T.K. Lundell, R. Floris, T. Glu moff and K.H. Winterhalter *et al.*, 1994a. Do carbohydrates play a role in the lignin peroxidase cycle? Redox catalysis in the endergonic region of the driving force. *Bioorganic Med. Chem.*, 2: 509-519. DOI: 10.1016/0968-0896(94)80021-9
- Sinsabaugh, R.L., 2010. Phenol oxidase, peroxidase and organic matter dynamics of soil. *Soil Biol. Biochem.*, 42: 391-404. DOI: 10.1016/j.soilbio.2009.10.014
- Smith, A.M., W.L. Morrison and P.J. Milham, 1982. Oxidation of indole-3-acetic acid by peroxidase: Involvement of reduced peroxidase and compound III with superoxide as a product. *Biochemistry*, 21: 4414-4419. DOI: 10.1021/bi00261a034
- Smith, A.T., S.A. Sanders, R.N. Thorneley, J.F. Burke and R.R. Bray, 1992. Characterisation of a haem active-site mutant of horseradish peroxidase, Phe41---Val, with altered reactivity towards hydrogen peroxide and reducing substrates. *Eur. J. Biochem.*, 207: 507-519. DOI: 10.1111/j.1432-1033.1992.tb17077.x
- Snook, M.E. and G.A. Hamilton, 1974. Oxidation and fragmentation of some phenyl-substituted alcohols and ethers by peroxydisulfate and Fenton's reagent. *J. Am. Chem. Soc.*, 96: 860-869. DOI: 10.1021/ja00810a035
- Stöcker, M., 2008. Bio- und BTL-Kraftstoffe in der Bioraffinerie: Katalytische Umwandlung Lignocellulose-reicher Biomasse mit porösen Stoffen. *Angewandte Chem.*, 120: 9340-9351. DOI: 10.1002/ange.200801476
- Tamura, M. and I. Yamazaki, 1972. Reactions of the oxyform of horseradish peroxidase. *J. Biochem.*, 71: 311-319. PMID: 5016264
- Tien, M. and T.K. Kirk, 1984. Lignin-degrading enzyme from *Phanerochaete chrysosporium*: Purification, characterization and catalytic properties of a unique H<sub>2</sub>O<sub>2</sub>-requiring oxygenase. *PNAS*, 81: 2280-2284. DOI:10.1073/pnas.81.8.2280
- Tien, M., 1987. Properties of Ligninase from *Phanerochaete Chrysosporium* and their possible applications. *Critical Rev. Microbiol.*, 15: 141-168. DOI: 10.3109/10408418709104456
- Torres, E. and M. Ayala, 2010. *Biocatalysis Based on Heme Peroxidases*. 1st Edn., Springer, ISBN-10: 3642126278, pp: 325.
- Valderrama, B. and R. Vazquez-Duhalt, 2005. Electronbalance during the oxidative self-inactivation of cytochrome c. *J. Mol. Catalysis B: Enzymatic*, 35: 41-44. DOI: 10.1016/j.molcatb.2005.05.003
- Valderrama, B., M. Ayala and R. Vazquez-Duhalt, 2002. Suicide inactivation of peroxidases and the challenge of engineering more robust enzymes. *Chem. Biol.*, 9: 555-565. DOI: 10.1016/S1074-5521(02)00149-7
- van Rantwijk, F. and R.A. Sheldon, 2000. Selective oxygen transfer catalysed by heme peroxidases: Synthetic and mechanistic aspects. *Curr. Opinion Biotechnol.*, 11: 554-564. DOI: 10.1016/S0958-1669(00)00143-9
- Villas-Bôas, S.G., E. Esposito and D.A. Mitchell, 2002. Microbial conversion of lignocellulosic residues for production of animal feeds. *Ani. Feed Sci. Technol.*, 98: 1-12. DOI: 10.1016/S0377-8401(02)00017-2
- Vlasits, J., C. Jakopitsch, M. Bernroither, M. Zamocky, P.G. Furtmuller and C. Obinger, 2010. Mechanisms of catalase ctivity of heme peroxidases. *Arch. Biochem. Biophys.*, 500: 74-81. DOI: 10.1016/j.abb.2010.04.018
- Wang, Y., R. Vazquez-Duhalt and M.A. Pickard, 2003. Manganese-lignin peroxidase hybrid from *Bjerkandera adusta* oxidizes polycyclic aromatic hydrocarbons more actively in the absence of manganese. *Canadian J. Microbiol.*, 49: 675-682. DOI: 10.1139/w03-091
- Wariishi, H. and M.H. Gold, 1990. Lignin peroxidase compound III. Mechanism of formation and decomposition. *J. Biol. Chem.*, 265: 2070-2077. PMID: 2298739
- Wong, D.W., 2009. Structure and action mecha nism of ligninolytic enzymes. *Applied Biochem. Biotechnol.*, 157: 174-209. DOI: 10.1007/s12010-008- 8279-z
- Yokota, K. and I. Yamazaki, 1965. The activity of the horseradish peroxidase compound 3. *Biochem. Biophys. Res. Commun.*, 18: 48-53. DOI: 10.1016/0006-291X(65)90880-6